Electronic Supplementary Material (ESI) for Organic and Biomolecular Chemistry

SUPPORTING INFORMATION

for

Laser flash photolysis study on retinol radical cation in polar solvents

Ali El-Agamey[*a,b]* and Shunichi Fukuzumi*[*a,c]*

[a]Department of Material and Life Science, Graduate School of Engineering, Osaka University, ALCA, Japan Science and Technology Agency (JST), Suita, Osaka 565-0871, Japan; [b]Chemistry Department, Faculty of Science, Mansoura University, New Damietta, Damietta, Egypt; [c]Department of Bioinspired Science, Ewha Womans University, Seoul 120-750, Korea

*Corresponding authors: Ali El-Agamey (Osaka University); Shunichi Fukuzumi (Osaka University)

E-mails: a_el_agamey@yahoo.co.uk; fukuzumi@chem.eng.osaka-u.ac.jp Tel. No.: +81-0668797369; Fax No.: +81-0668797370

Contents

Fig. S8B Time profiles of absorbance at 580 and 370 nm obtained following LFP (355 nm) of retinol (4.5×10^{-5} M) in air-saturated acetonitrile (laser energy ~15 mJ).

Fig. S9A Transient absorption spectra obtained following LFP (355 nm) of retinyl acetate (Abs. at 355 nm ~0.8 in a 1 cm cell) in air-saturated methanol (laser energy ~15 mJ).

Fig. S9B Time profiles of absorbance at 580 and 370 nm obtained following LFP (355 nm) of retinyl acetate (Abs. at 355 nm ~0.8 in a 1 cm cell) in air-saturated methanol (laser energy ~15 mJ).

Fig. S10A Transient absorption spectra obtained following LFP (355 nm) of retinyl acetate (Abs. at 355 nm ~0.8 in a 1 cm cell) in air-saturated acetonitrile (laser energy ~15 mJ).

Fig. S10B Time profiles of absorbance at 580 and 370 nm obtained following LFP (355 nm) of retinyl acetate (Abs. at 355 nm ~0.8 in a 1 cm cell) in air-saturated acetonitrile (laser energy ~15 mJ).

Fig. S11 Normalized time profiles of absorbance at 580 nm obtained following LFP (355 nm) of retinol (4.5×10^{-5} M) and retinyl acetate (Abs. at 355 nm ~0.8 in a 1 cm cell) in air-saturated acetonitrile (laser energy ~15 mJ).

Fig. S12 Time profiles of absorbance at 580 and 380 nm obtained following LFP (355 nm) of retinyl acetate (Abs. at 355 nm ~0.8 in a 1 cm cell) and tetra-*n*-butylammonium bromide (1.0×10^{-4} M) in air-saturated acetonitrile (laser energy ~15 mJ).

Fig. S13 Plots of pseudo-first-order rate constants (k_{obs}) for the decay of the absorbance at 580 nm, obtained following LFP (355 nm) of retinol (4.5×10^{-5} M) and retinyl acetate (Abs. at 355 nm ~0.8 in a 1 cm cell) in air-saturated benzonitrile (laser energy ~25 mJ), *versus* tetra-*n*-butylammonium bromide concentration.

Fig. S14A Plots of pseudo-first-order rate constants (k_{obs}) for the decay of the transient profiles at 580 nm, obtained following LFP (355 nm) of retinol (4.5×10^{-5} M) and retinyl acetate (Abs. at 355 nm ~0.8 in a 1 cm cell) in air-saturated acetonitrile (laser energy ~15 mJ), *versus* tetra-*n*-butylammonium chloride concentration.

Fig. S14B Plots of pseudo-first-order rate constants (k_{obs}) for the decay of the transient profiles at 580 nm, obtained following LFP (355 nm) of retinol (4.5×10^{-5} M) and retinyl acetate (Abs. at 355 nm ~0.8 in a 1 cm cell) in air-saturated benzonitrile (laser energy ~25 mJ), *versus* tetra-*n*-butylammonium chloride concentration.

Fig. S15A Time profiles of absorbance at 580 and 380 nm obtained following LFP (355 nm) of retinol (4.5×10^{-5} M) and tetra-*n*-butylammonium bromide (5×10^{-5} M) in air-saturated benzonitrile (laser energy ~25 mJ).

Fig. S15B Time profiles of absorbance at 580 and 380 nm obtained following LFP (355 nm) of retinyl acetate (Abs. at 355 nm ~0.8 in a 1 cm cell) and tetra-*n*-butylammonium bromide (5×10^{-5} M) in air-saturated benzonitrile (laser energy ~25 mJ).

Fig. S15C Time profiles of absorbance at 580 and 390 nm obtained following LFP (355 nm) of retinol (4.5×10^{-5} M) and tetra-*n*-butylammonium chloride (4×10^{-5} M) in air-saturated benzonitrile (laser energy ~25 mJ).

Fig. S15D Time profiles of absorbance at 580 and 390 nm obtained following LFP (355 nm) of retinyl acetate (Abs. at 355 nm ~0.8 in a 1 cm cell) and tetra-*n*-butylammonium chloride (4×10^{-5} M) in air-saturated benzonitrile (laser energy ~25 mJ).

Fig. S16A Time profiles of absorbance at 580 and 370 nm obtained following LFP (355 nm) of retinol (4.5×10^{-5} M) and tetra-*n*-butylammonium bromide (1×10^{-5} M) in air-saturated acetone (laser energy ~25 mJ).

Fig. S16B Plot of pseudo-first-order rate constants (k_{obs}) for the decay of the transient profiles at 580 nm, obtained following LFP (355 nm) of retinol (4.5×10^{-5} M) in air-saturated acetone (laser energy ~25 mJ), *versus* tetra-*n*-butylammonium bromide concentration.

Fig. S17 Time profiles of absorbance at 580 nm obtained following LFP (355 nm) of retinol (4.5×10^{-5} M) and retinyl acetate (Abs. at 355 nm ~0.8 in a 1 cm cell) in the presence of tetra-*n*-butylammonium chloride (0.12 M) in air-saturated methanol (laser energy ~15 mJ).

Fig. S18 Normalized transient absorption spectra of $APO^{\bullet+}$ obtained following LFP (355 nm) of (1) retinol (5.0×10^{-5} M) and APO (1.5×10^{-4} M) after 7 μs (laser energy ~25 mJ) or (2) 1,4-dicyanonaphthalene (5.0×10^{-3} M), biphenyl (0.30 M) and APO (1.5×10^{-4} M) after 15 μs (laser energy ~10 mJ) in air-saturated benzonitrile.

Fig. S19 Plots of absorbance at 580 nm *versus* incident laser energy obtained following direct excitation (355 nm) of retinol (4.5×10^{-5} M) in air-saturated methanol, benzonitrile and aqueous 2% Triton X-100.

Fig. S20 Time profiles of absorbance at 580 and 980 nm obtained following LFP (355 nm) of retinol (4.5×10^{-5} M) in the presence of β-CAR (5.0×10^{-5} M) in air-saturated benzonitrile (laser energy ~40 mJ).

Fig. S21 Time profiles of absorbance at (A) 580 and 910 nm obtained following LFP (355 nm) of retinol (4.5×10^{-5} M) in the presence of ZEA (1.5×10^{-5} M) in air-saturated methanol (laser energy ~20 mJ) and (B) those at 580 and 980 nm obtained following LFP (355 nm) of retinol (4.5×10^{-5} M) in the presence of ZEA (4.5×10^{-5} M) in air-saturated benzonitrile (laser energy ~30 mJ).

Fig. S22 Time profiles of absorbance at (A) 580 and 820 nm obtained following LFP (355 nm) of retinol (4.5×10^{-5} M) in the presence of APO (7×10^{-5} M) in air-saturated methanol (laser energy ~15 mJ) and (B) those at 580 and 820 nm obtained following LFP (355 nm) of retinol (4.5×10^{-5} M) in the presence of APO (1.6×10^{-4} M) in air-saturated benzonitrile (laser energy ~30 mJ).

Fig. S23 Plots of pseudo-first-order rate constants (k_{obs}) for the decay of the transient profiles at 580 nm, obtained following LFP (355 nm) of retinol (4.5×10^{-5} M) in air-saturated methanol (laser energy ~10 mJ) or benzonitrile (laser energy ~25 mJ), *versus* ASTA concentration.

Fig. S24 Plot of pseudo-first-order rate constants (k_{obs}) for the decay of the transient profiles at 580 nm, obtained following LFP (355 nm) of retinol (4.5×10^{-5} M) in air-saturated benzonitrile (laser energy ~40 mJ), *versus* β-CAR concentration.

Fig. S25 Plots of pseudo-first-order rate constants (k_{obs}) for the decay of the transient profiles at 580 nm, obtained following LFP (355 nm) of retinol (4.5×10^{-5} M) in air-saturated methanol (laser energy ~20 mJ) or benzonitrile (laser energy ~30 mJ), *versus* ZEA concentration.

Fig. S26 Plots of pseudo-first-order rate constants (k_{obs}) for the decay of the transient profiles at 580 nm, obtained following LFP (355 nm) of retinol (4.5×10^{-5} M) in air-saturated methanol (laser energy ~15 mJ) or benzonitrile (laser energy ~30 mJ), *versus* APO concentration.

Fig. S27 Transient spectra obtained following LFP (355 nm) of retinol (4.5×10^{-5} M) and pyridine (1.0 M) in air-saturated methanol (laser energy ~15 mJ).

Fig. S28 Plots of pseudo-first-order rate constants (k_{obs}) for the decay of the transient profiles at 580 nm, obtained following LFP (355 nm) of retinol (4.5×10^{-5} M) in air-saturated methanol (laser energy ~20 mJ), *versus* pyridine derivative concentration.

Fig. S29 Transient absorption spectra obtained following LFP (355 nm) of retinol (~1.0×10^{-4} M) in air-saturated aqueous 2% Triton X-100 (laser energy ~15 mJ).

Fig. S30A Transient absorption spectra obtained following LFP (355 nm) of retinol (4.5×10^{-5} M) and pyridine (1.0 M) in air-saturated aqueous 2% Triton X-100 (laser energy ~20 mJ).

Fig. S30B Time profiles of absorbance at 580 and 380 nm obtained following LFP (355 nm) of retinol (4.5×10^{-5} M) and pyridine (1.0 M) in air-saturated aqueous 2% Triton X-100 (laser energy ~20 mJ).

Fig. S31 Plots of pseudo-first-order rate constants (k_{obs}) for the decay of the absorbance at 580 nm, obtained following LFP (355 nm) of retinol (4.5×10^{-5} M) in air-saturated benzonitrile (laser energy ~25 mJ), *versus* pyridine derivative concentration.

Fig. S32 Plots of pseudo-first-order rate constants (k_{obs}) for the decay of the absorbance at 580 nm, obtained following LFP (355 nm) of retinol (4.5×10^{-5} M) in air-saturated methanol (laser energy ~10 mJ) or benzonitrile (laser energy ~20 mJ), *versus* 2,6-dimethylpyridine concentration.

Fig. S33A Time profiles of absorbance at 580 and 370 nm obtained following LFP (355 nm) of retinol (4.5×10^{-5} M) and 2-aminopyridine (0.2 M) in air-saturated methanol (laser energy ~20 mJ).

Fig. S33B Time profiles of absorbance at 580 and 370 nm obtained following LFP (355 nm) of retinol (4.5×10^{-5} M) and 4-aminopyridine (0.25 M) in air-saturated methanol (laser energy ~20 mJ).

Fig. S34A Time profiles of absorbance at 580 and 380 nm obtained following LFP (355 nm) of retinol (4.5×10^{-5} M) and 2-aminopyridine (0.06 M) in air-saturated benzonitrile (laser energy ~20 mJ).

Fig. S34B Time profiles of absorbance at 580 and 380 nm obtained following LFP (355 nm) of retinol (4.5×10^{-5} M) and 2,6-dimethylpyridine (2.0 M) in air-saturated benzonitrile (laser energy ~20 mJ).

Fig. S35 Time profiles of absorbance at 580 nm obtained following LFP (355 nm) of (a) retinol (4.5×10^{-5} M) or (b) retinol (4.5×10^{-5} M) and 2-cyanopyridine (1.0 M) in air-saturated methanol (laser energy ~20 mJ).

Fig. S36 Time profiles of absorbance at 580 and 380 nm obtained following LFP (355 nm) of retinol (4.5×10^{-5} M) in air-saturated aqueous 2% Triton X-100 at pH = 10.5 (laser energy ~25 mJ).

Fig. S37A Normalized time profiles of absorbance at 580 nm obtained following LFP (355 nm) of retinol (4.5×10^{-5} M) and retinyl acetate (Abs. at 355 nm ~0.8 in a 1 cm cell) in the presence of pyridine (1.0 M) in air-saturated methanol (laser energy ~15 mJ).

Fig. S37B Normalized time profiles of absorbance at 580 nm obtained following LFP (355 nm) of retinol (4.5×10^{-5} M) and retinyl acetate (Abs. at 355 nm ~0.8 in a 1 cm cell) in the presence of pyridine (1.0 M) in air-saturated acetonitrile (laser energy ~15 mJ).

Scheme S1

Scheme S2

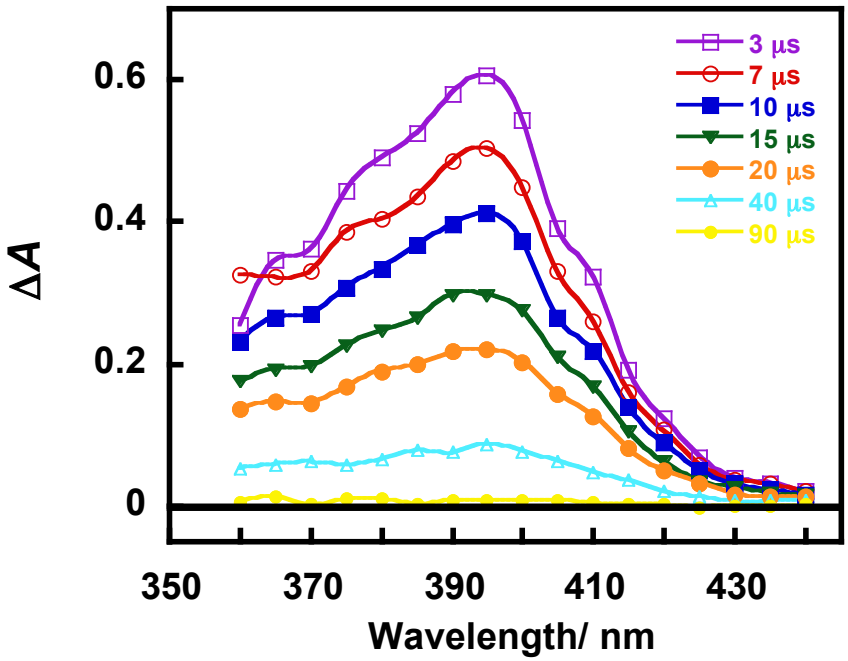

Fig. S1 Transient spectra obtained following LFP (266 nm) of naphthalene (Abs. at 266 nm ~2.4 in a 1 cm cell) and retinol (~1 × 10^{-4} M) in argon-saturated methanol (laser energy ~5 mJ) (See eqn (S1)).[a]

$$^{3}\text{Naph} + \text{Retinol} \longrightarrow \text{Naph} + {}^{3}\text{Retinol} \quad \text{(S1)}$$

[a]For the nanosecond laser flash photolysis at 266 nm, Nd:YAG laser (Continuum, SLI-20, 4–6 ns fwhm) was used.

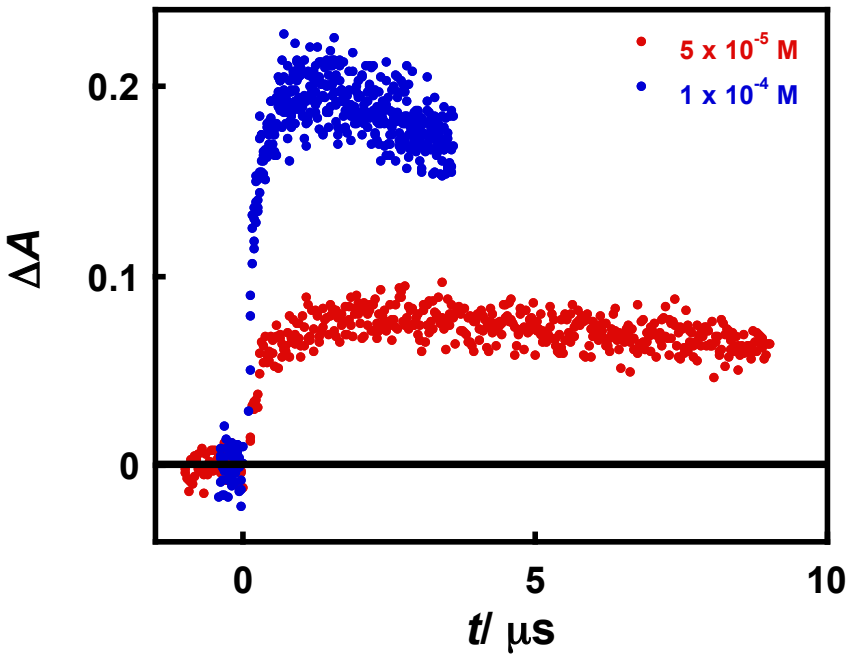

Fig. S2 The influence of retinol concentration on the rate of the transient growth at 370 nm, obtained following LFP (355 nm) of retinol in argon-saturated methanol (laser energy ~15 mJ).

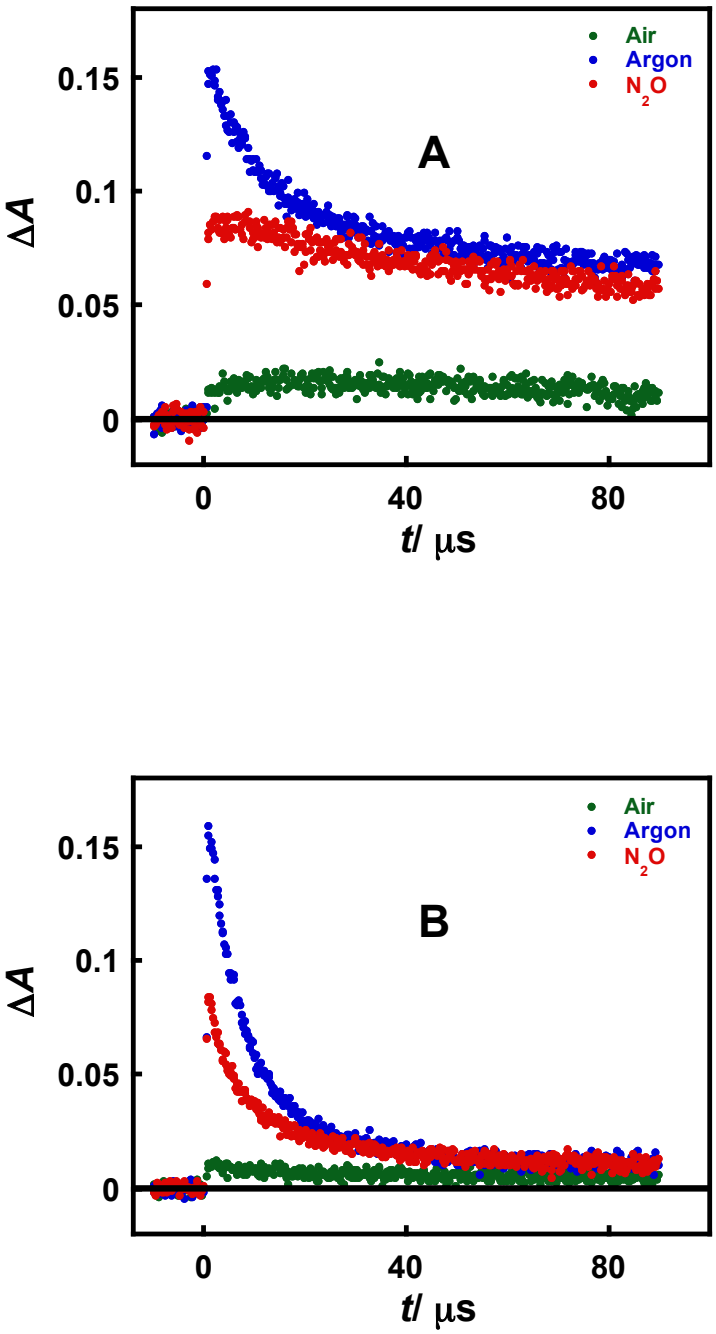

Fig. S3 Time profiles of absorbance at (A) 370 nm and (B) 400 nm, obtained following LFP (355 nm) of retinol (~1 × 10^{-4} M) in air, argon and N_2O-saturated methanol (laser energy ~15 mJ).

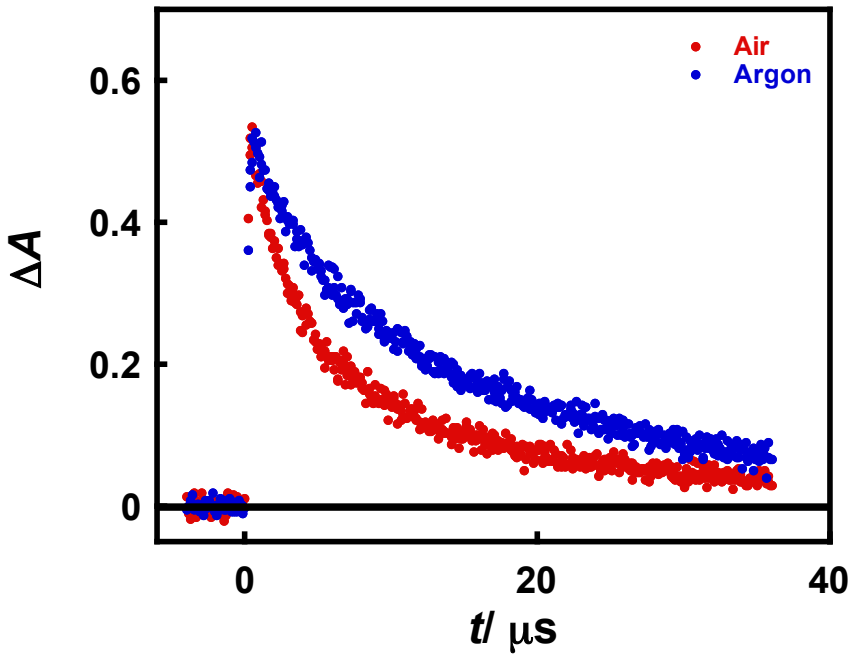

Fig. S4 Time profiles of absorbance at 580 nm, obtained following LFP (355 nm) of retinol (~1 × 10^{-4} M) in air and argon-saturated methanol (laser energy ~15 mJ).

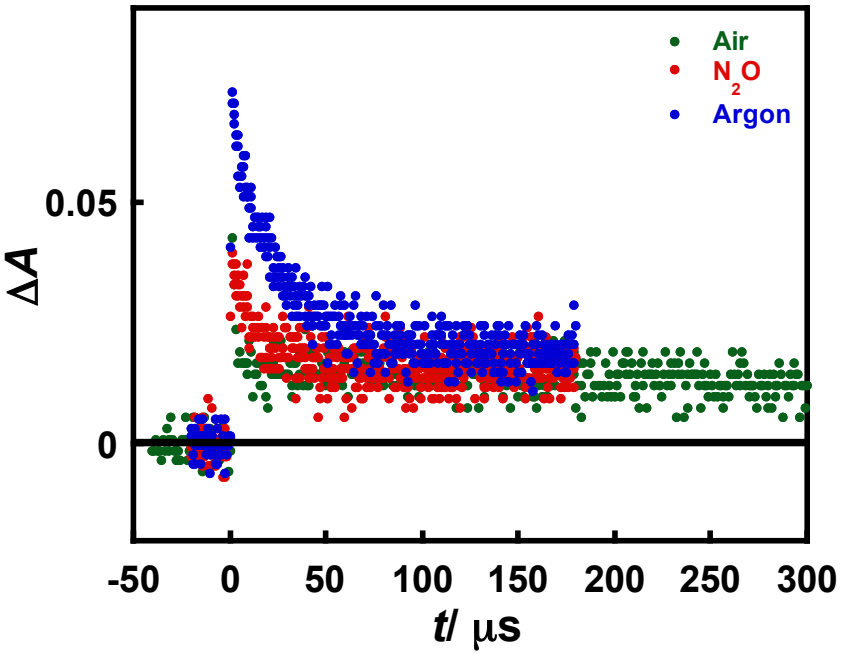

Fig. S5 Time profiles of absorbance at 380 nm, obtained following LFP (355 nm) of retinol (~1 × 10^{-4} M) in air, argon and N_2O-saturated aqueous 2% Triton X-100 (laser energy ~15 mJ).

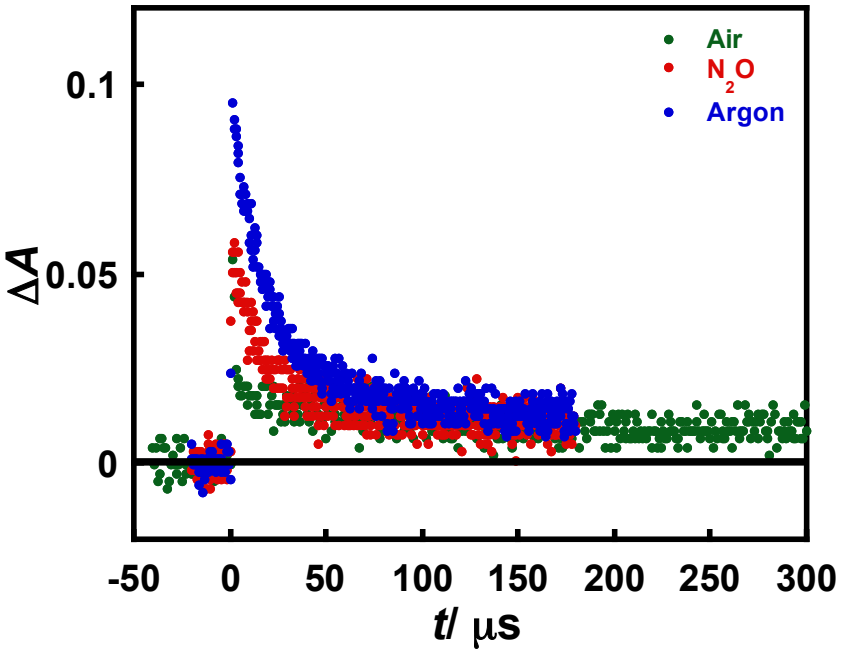

Fig. S6 Time profiles of absorbance at 400 nm, obtained following LFP (355 nm) of retinol (~1 × 10^{-4} M) in air, argon and N_2O-saturated aqueous 2% Triton X-100 (laser energy ~15 mJ).

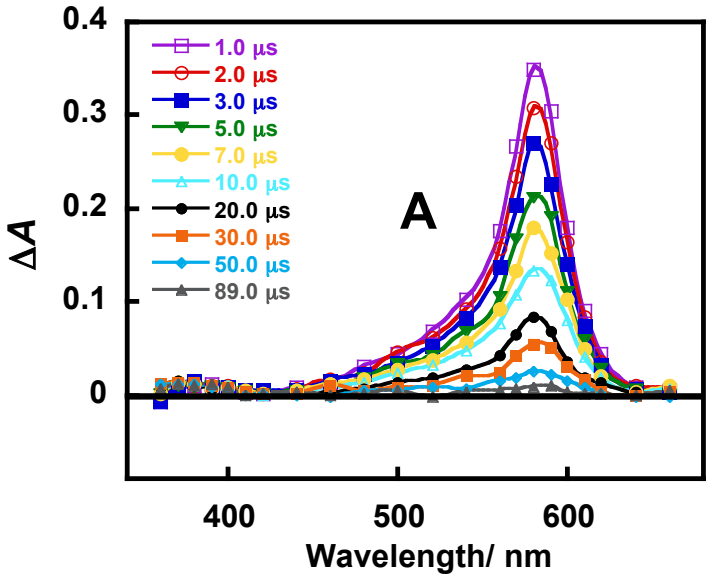

Fig. S7A Transient absorption spectra obtained following LFP (355 nm) of retinol (4.5×10^{-5} M) in air-saturated methanol (laser energy ~15 mJ).

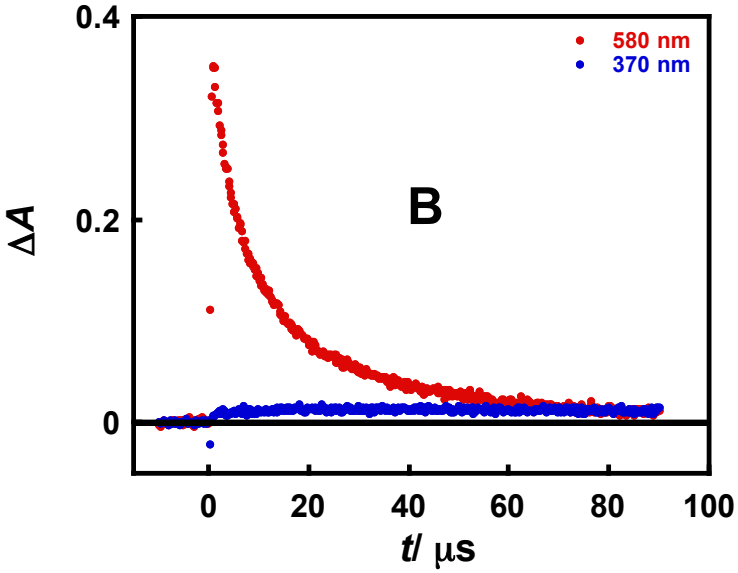

Fig. S7B Time profiles of absorbance at 580 and 370 nm obtained following LFP (355 nm) of retinol (4.5×10^{-5} M) in air-saturated methanol (laser energy ~15 mJ).

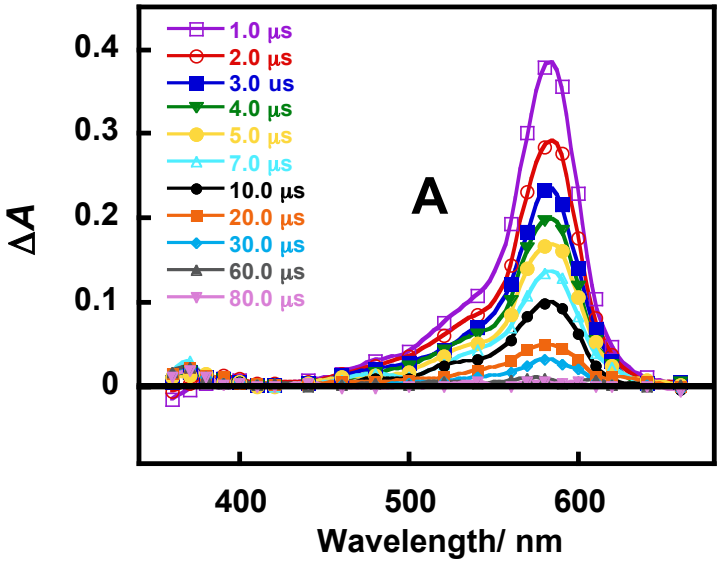

Fig. S8A Transient absorption spectra obtained following LFP (355 nm) of retinol (4.5×10^{-5} M) in air-saturated acetonitrile (laser energy ~15 mJ).

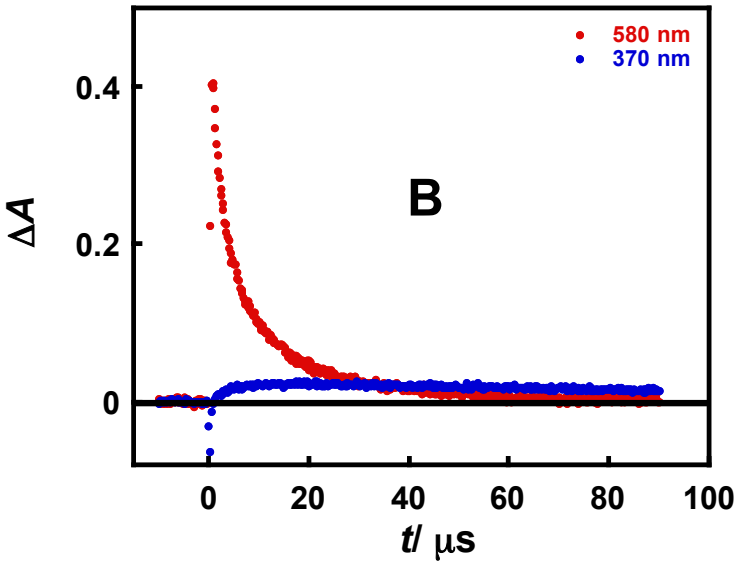

Fig. S8B Time profiles of absorbance at 580 and 370 nm obtained following LFP (355 nm) of retinol (4.5×10^{-5} M) in air-saturated acetonitrile (laser energy ~15 mJ).

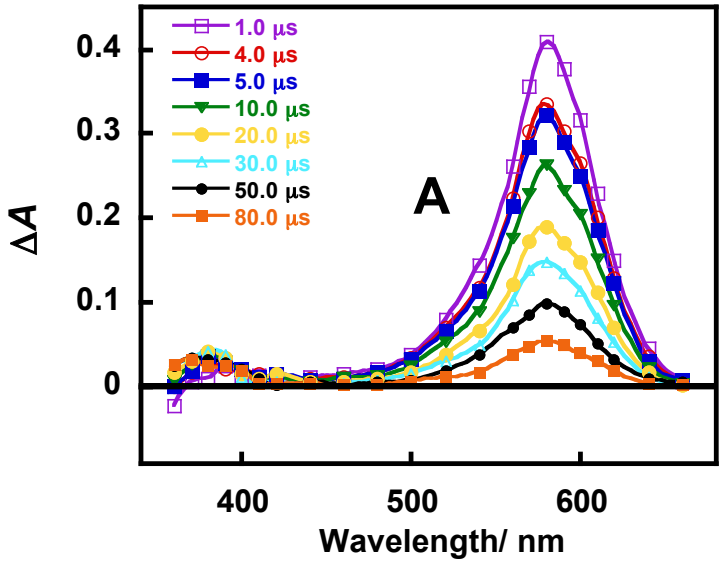

Fig. S9A Transient absorption spectra obtained following LFP (355 nm) of retinyl acetate (Abs. at 355 nm ~0.8 in a 1 cm cell) in air-saturated methanol (laser energy ~15 mJ).

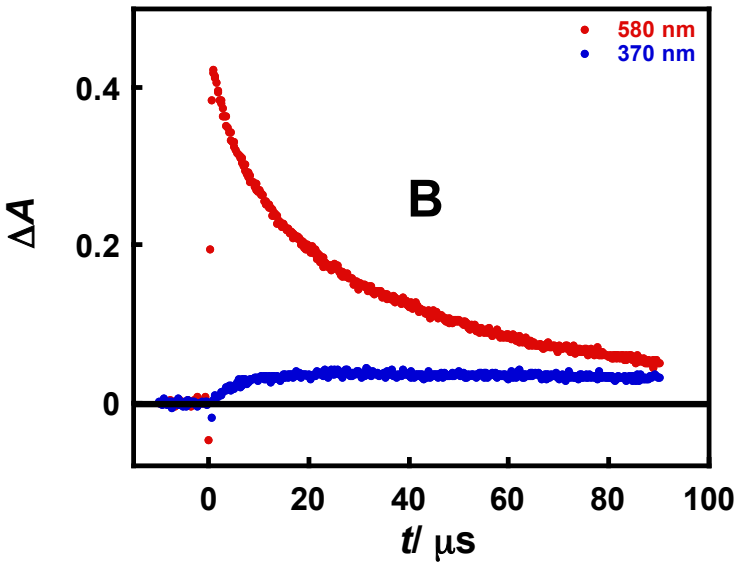

Fig. S9B Time profiles of absorbance at 580 and 370 nm obtained following LFP (355 nm) of retinyl acetate (Abs. at 355 nm ~0.8 in a 1 cm cell) in air-saturated methanol (laser energy ~15 mJ).

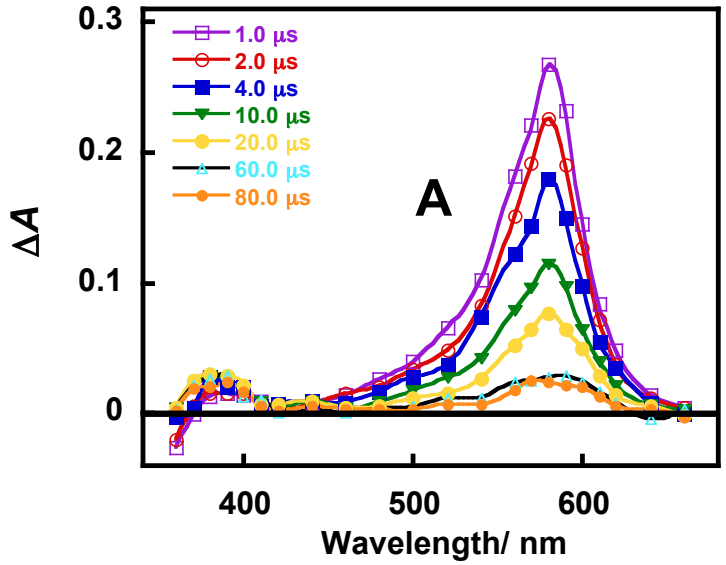

Fig. S10A Transient absorption spectra obtained following LFP (355 nm) of retinyl acetate (Abs. at 355 nm ~0.8 in a 1 cm cell) in air-saturated acetonitrile (laser energy ~15 mJ).

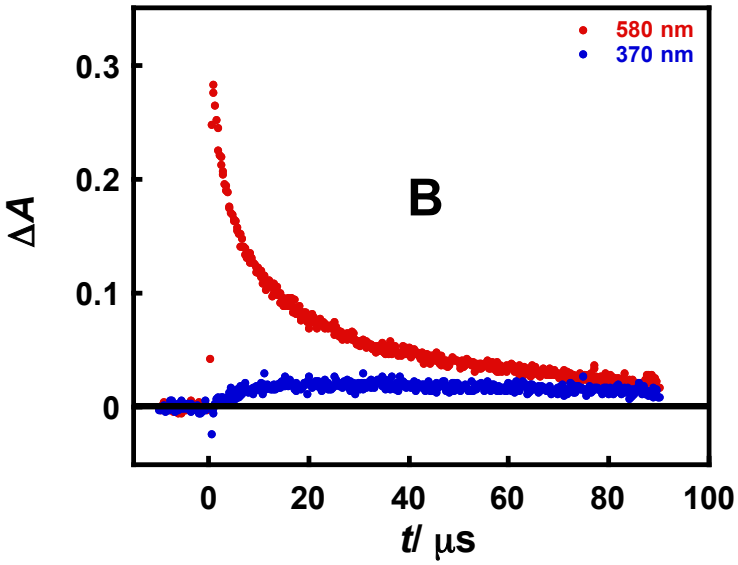

Fig. S10B Time profiles of absorbance at 580 and 370 nm obtained following LFP (355 nm) of retinyl acetate (Abs. at 355 nm ~0.8 in a 1 cm cell) in air-saturated acetonitrile (laser energy ~15 mJ).

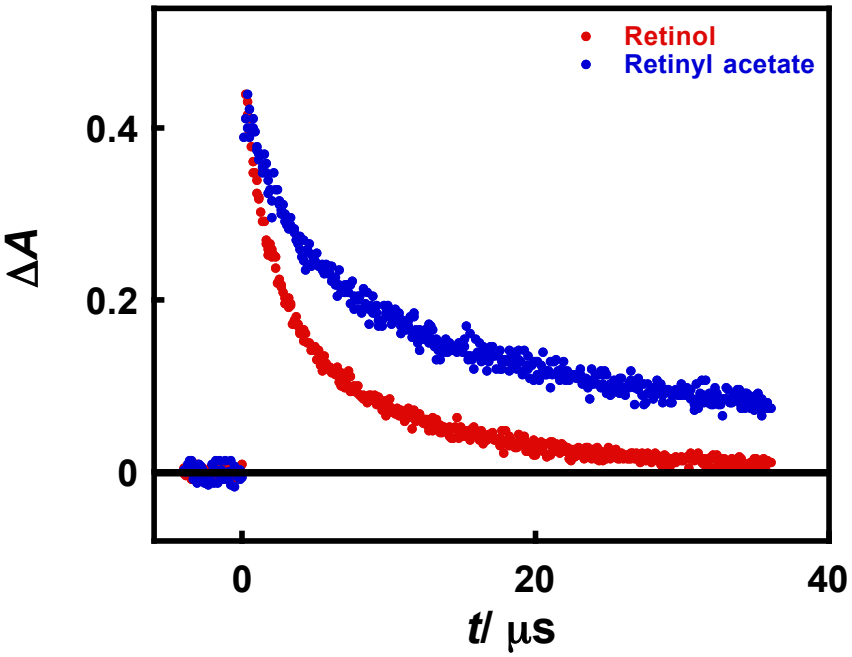

Fig. S11 Normalized time profiles of absorbance at 580 nm obtained following LFP (355 nm) of retinol (4.5×10^{-5} M) and retinyl acetate (Abs. at 355 nm ~0.8 in a 1 cm cell) in air-saturated acetonitrile (laser energy ~15 mJ).

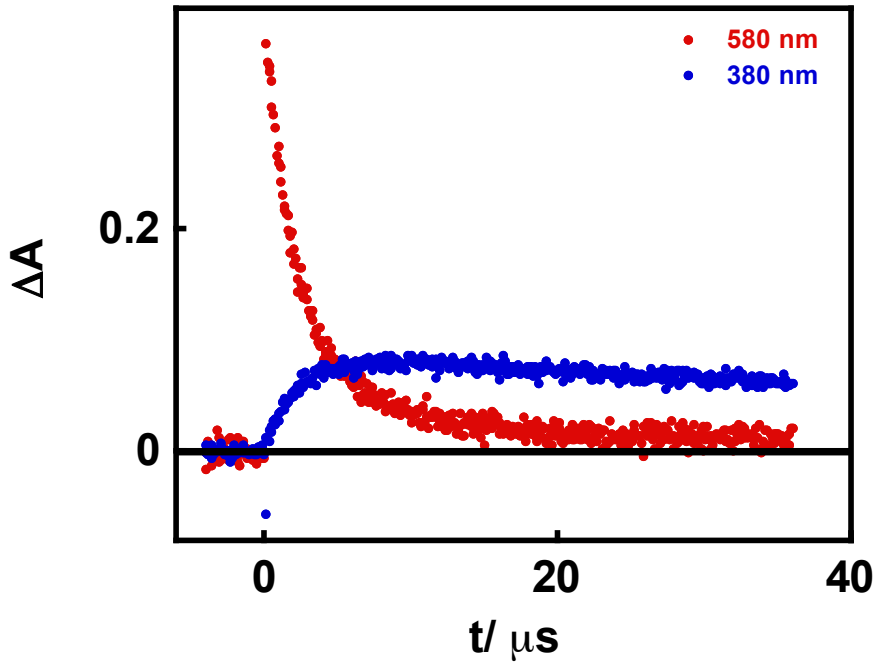

Fig. S12 Time profiles of absorbance at 580 and 380 nm obtained following LFP (355 nm) of retinyl acetate (Abs. at 355 nm ~0.8 in a 1 cm cell) and tetra-*n*-butylammonium bromide (1.0×10^{-4} M) in air-saturated acetonitrile (laser energy ~15 mJ).

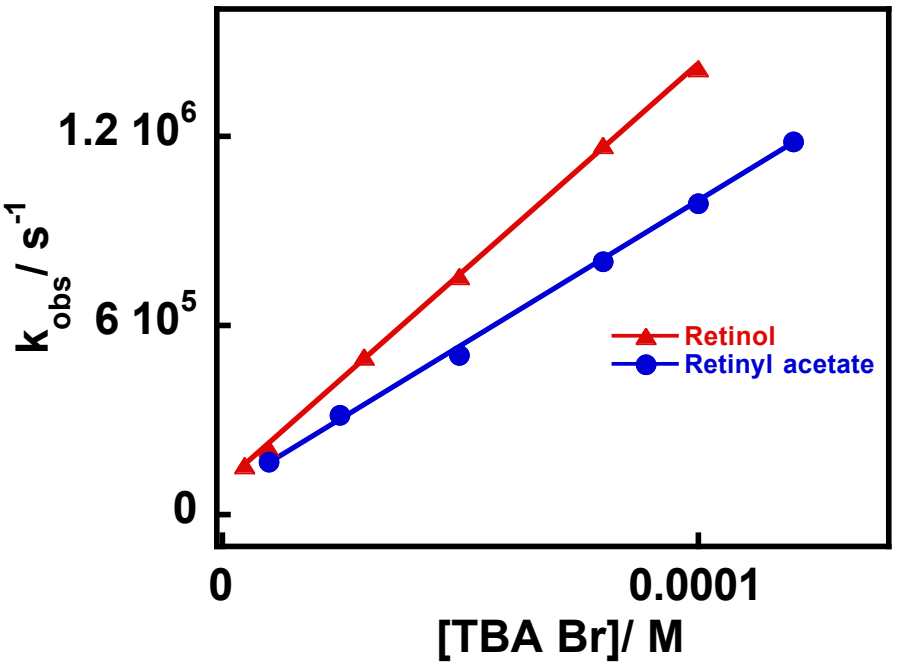

Fig. S13 Plots of pseudo-first-order rate constants (k_{obs}) for the decay of the absorbance at 580 nm, obtained following LFP (355 nm) of retinol (4.5×10^{-5} M) and retinyl acetate (Abs. at 355 nm ~0.8 in a 1 cm cell) in air-saturated benzonitrile (laser energy ~25 mJ), *versus* tetra-*n*-butylammonium bromide concentration.

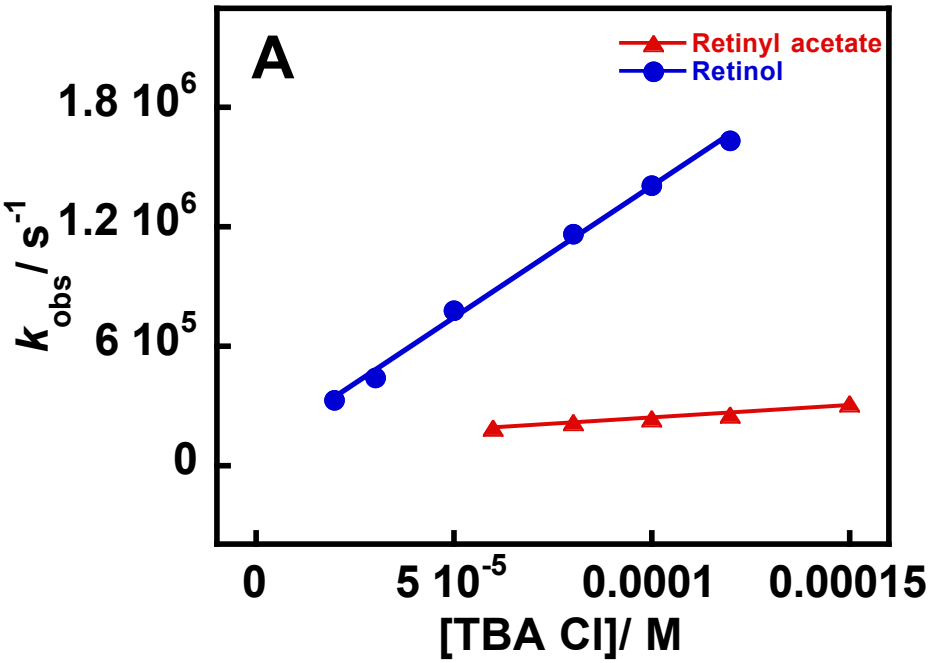

Fig. S14A Plots of pseudo-first-order rate constants (k_{obs}) for the decay of the transient profiles at 580 nm, obtained following LFP (355 nm) of retinol (4.5×10^{-5} M) and retinyl acetate (Abs. at 355 nm ~0.8 in a 1 cm cell) in air-saturated acetonitrile (laser energy ~15 mJ), *versus* tetra-*n*-butylammonium chloride concentration.

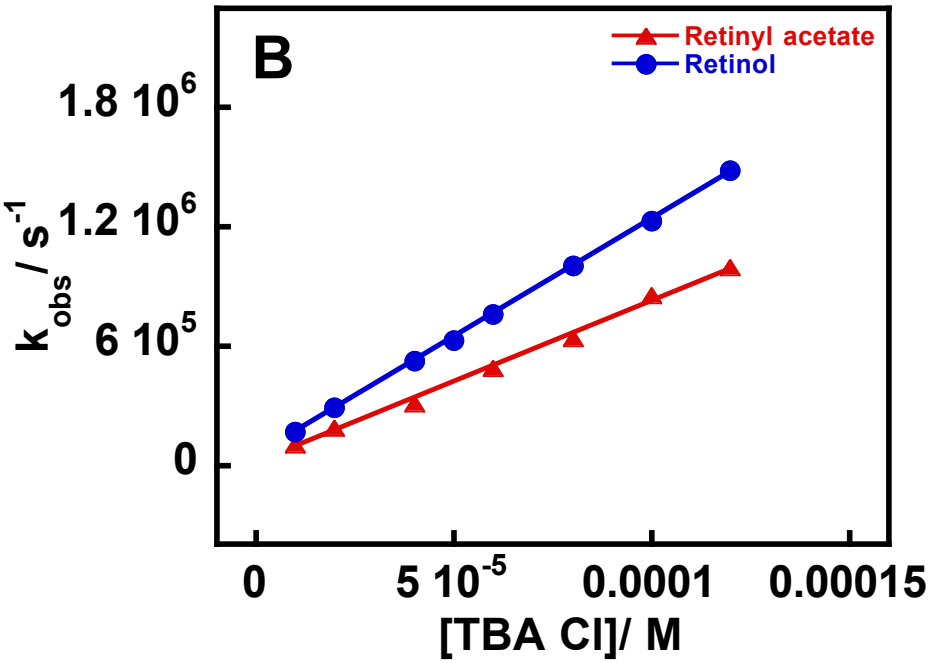

Fig. S14B Plots of pseudo-first-order rate constants (k_{obs}) for the decay of the transient profiles at 580 nm, obtained following LFP (355 nm) of retinol (4.5×10^{-5} M) and retinyl acetate (Abs. at 355 nm ~0.8 in a 1 cm cell) in air-saturated benzonitrile (laser energy ~25 mJ), *versus* tetra-*n*-butylammonium chloride concentration.

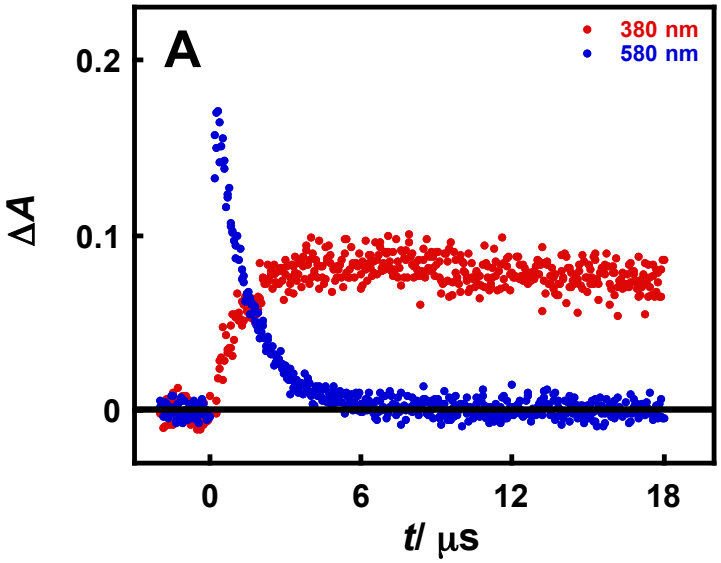

Fig. S15A Time profiles of absorbance at 580 and 380 nm obtained following LFP (355 nm) of retinol (4.5×10^{-5} M) and tetra-*n*-butylammonium bromide (5×10^{-5} M) in air-saturated benzonitrile (laser energy ~25 mJ).

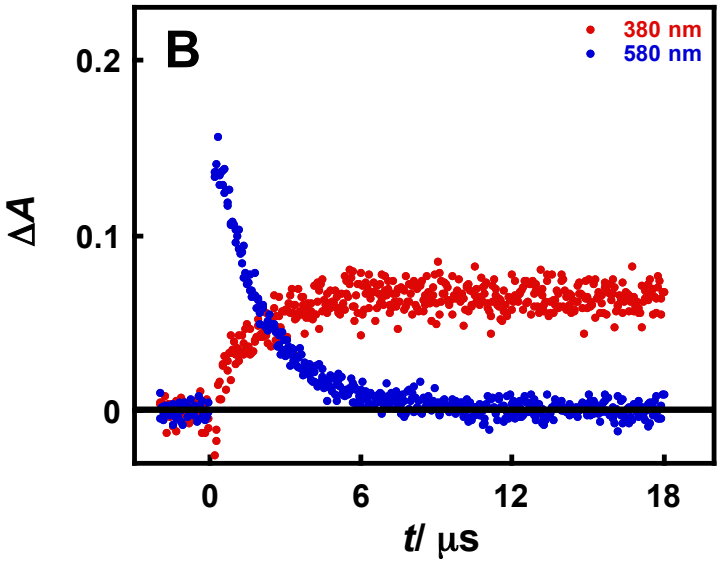

Fig. S15B Time profiles of absorbance at 580 and 380 nm obtained following LFP (355 nm) of retinyl acetate (Abs. at 355 nm ~0.8 in a 1 cm cell) and tetra-*n*-butylammonium bromide (5×10^{-5} M) in air-saturated benzonitrile (laser energy ~25 mJ).

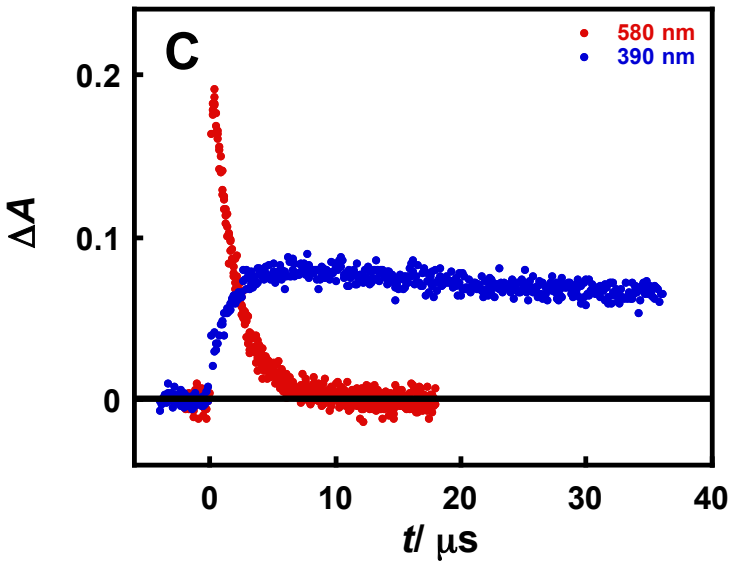

Fig. S15C Time profiles of absorbance at 580 and 390 nm obtained following LFP (355 nm) of retinol (4.5×10^{-5} M) and tetra-*n*-butylammonium chloride (4×10^{-5} M) in air-saturated benzonitrile (laser energy ~25 mJ).

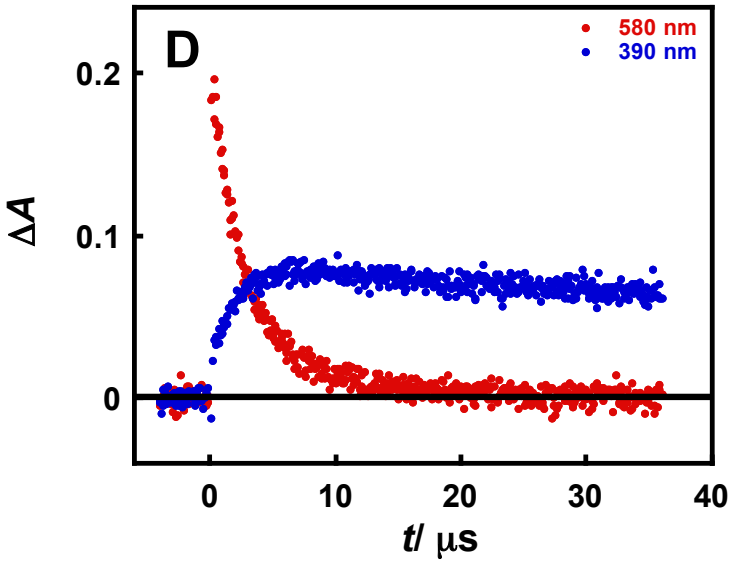

Fig. S15D Time profiles of absorbance at 580 and 390 nm obtained following LFP (355 nm) of retinyl acetate (Abs. at 355 nm ~0.8 in a 1 cm cell) and tetra-*n*-butylammonium chloride (4×10^{-5} M) in air-saturated benzonitrile (laser energy ~25 mJ).

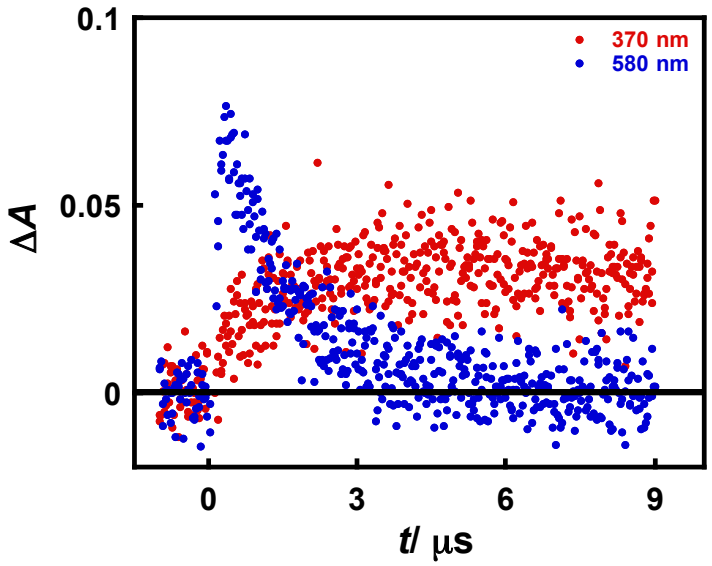

Fig. S16A Time profiles of absorbance at 580 and 370 nm obtained following LFP (355 nm) of retinol (4.5×10^{-5} M) and tetra-*n*-butylammonium bromide (1×10^{-5} M) in air-saturated acetone (laser energy ~25 mJ).

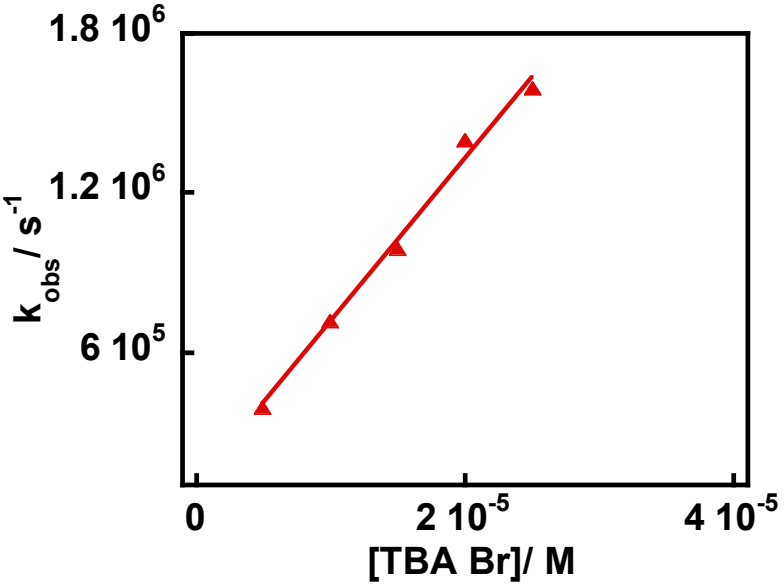

Fig. S16B Plot of pseudo-first-order rate constants (k_{obs}) for the decay of the transient profiles at 580 nm, obtained following LFP (355 nm) of retinol (4.5×10^{-5} M) in air-saturated acetone (laser energy ~25 mJ), *versus* tetra-*n*-butylammonium bromide concentration.

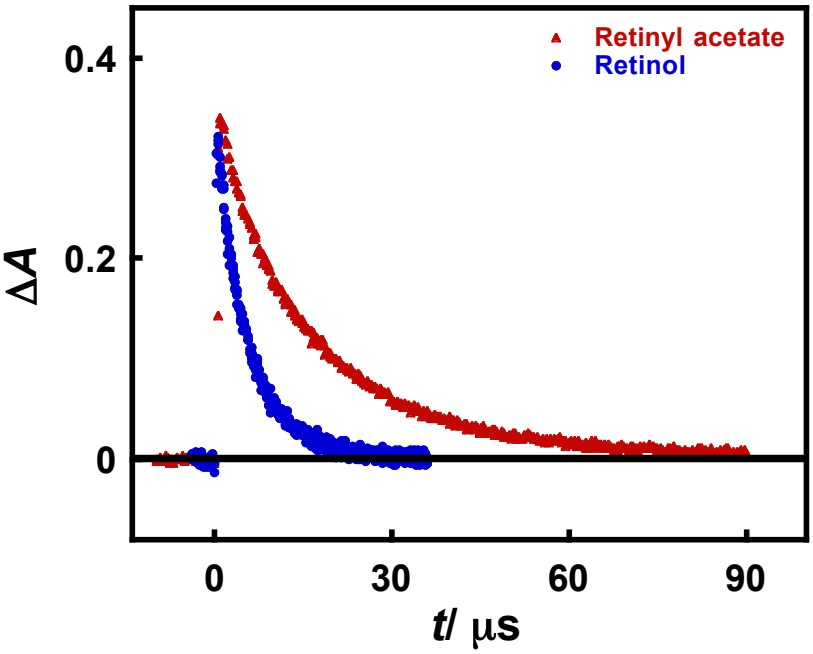

Fig. S17 Time profiles of absorbance at 580 nm obtained following LFP (355 nm) of retinol (4.5×10^{-5} M) and retinyl acetate (Abs. at 355 nm ~0.8 in a 1 cm cell) in the presence of tetra-*n*-butylammonium chloride (0.12 M) in air-saturated methanol (laser energy ~15 mJ).

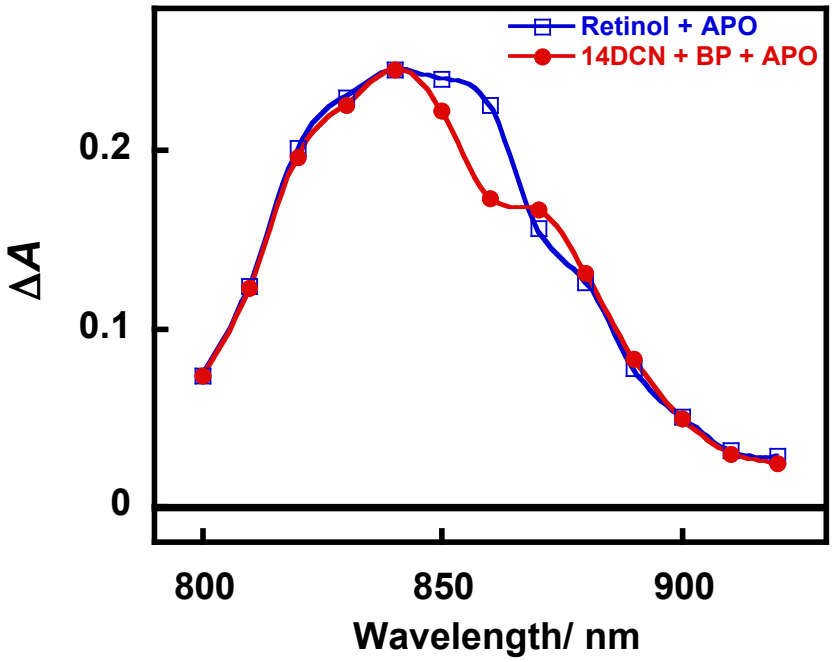

Fig. S18 Normalized transient absorption spectra of $APO^{\bullet+}$ obtained following LFP (355 nm) of (1) retinol (5.0×10^{-5} M) and APO (1.5×10^{-4} M) after 7 μs (laser energy ~25 mJ) or (2) 1,4-dicyanonaphthalene (5.0×10^{-3} M), biphenyl (0.30 M) and APO (1.5×10^{-4} M) after 15 μs (laser energy ~10 mJ) in air-saturated benzonitrile.

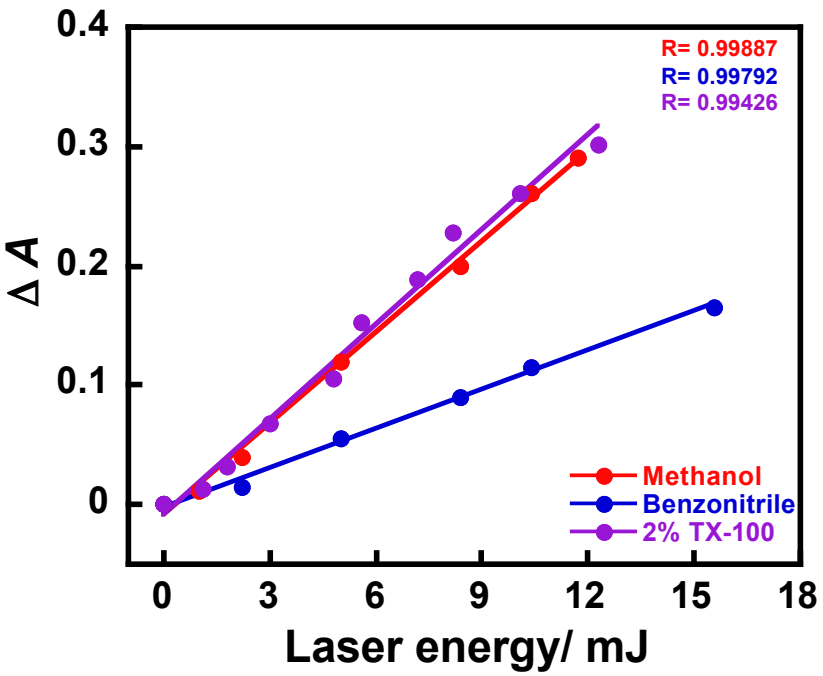

Fig. S19 Plots of absorbance at 580 nm *versus* incident laser energy obtained following direct excitation (355 nm) of retinol (4.5×10^{-5} M) in air-saturated methanol, benzonitrile and aqueous 2% Triton X-100.

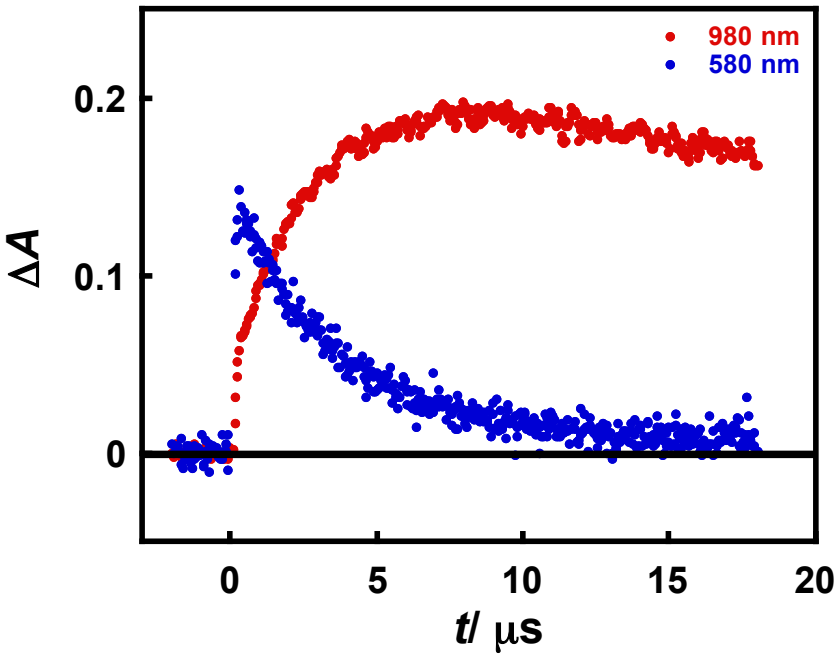

Fig. S20 Time profiles of absorbance at 580 and 980 nm obtained following LFP (355 nm) of retinol (4.5×10^{-5} M) in the presence of β-CAR (5.0×10^{-5} M) in air-saturated benzonitrile (laser energy ~40 mJ).

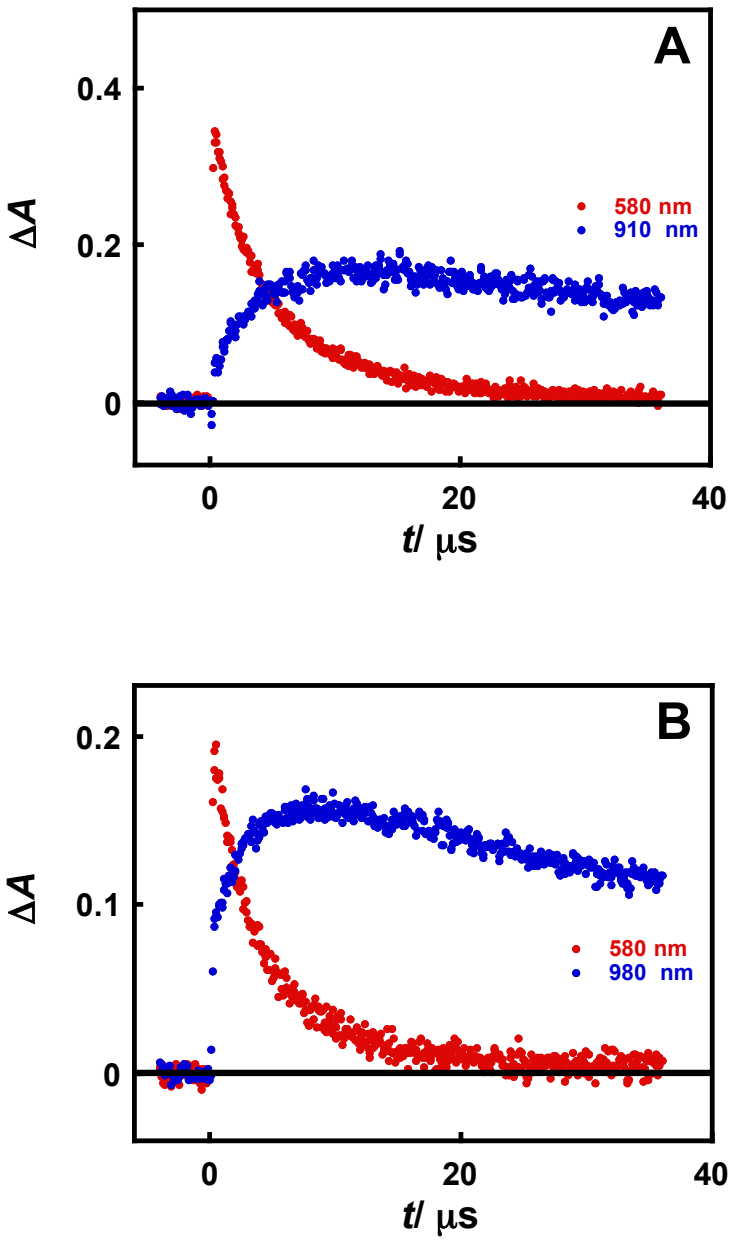

Fig. S21 Time profiles of absorbance at (A) 580 and 910 nm obtained following LFP (355 nm) of retinol (4.5×10^{-5} M) in the presence of ZEA (1.5×10^{-5} M) in air-saturated methanol (laser energy ~20 mJ) and (B) those at 580 and 980 nm obtained following LFP (355 nm) of retinol (4.5×10^{-5} M) in the presence of ZEA (4.5×10^{-5} M) in air-saturated benzonitrile (laser energy ~30 mJ).

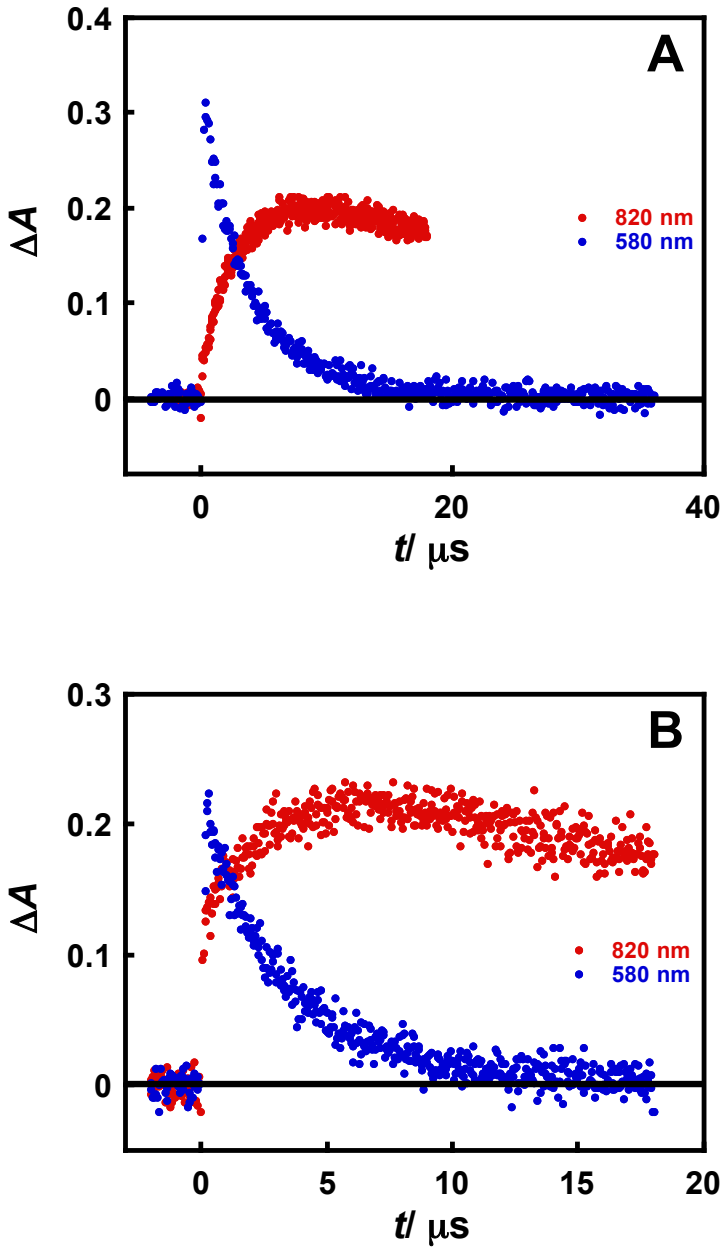

Fig. S22 Time profiles of absorbance at (A) 580 and 820 nm obtained following LFP (355 nm) of retinol (4.5×10^{-5} M) in the presence of APO (7×10^{-5} M) in air-saturated methanol (laser energy ~15 mJ) and (B) those at 580 and 820 nm obtained following LFP (355 nm) of retinol (4.5×10^{-5} M) in the presence of APO (1.6×10^{-4} M) in air-saturated benzonitrile (laser energy ~30 mJ).

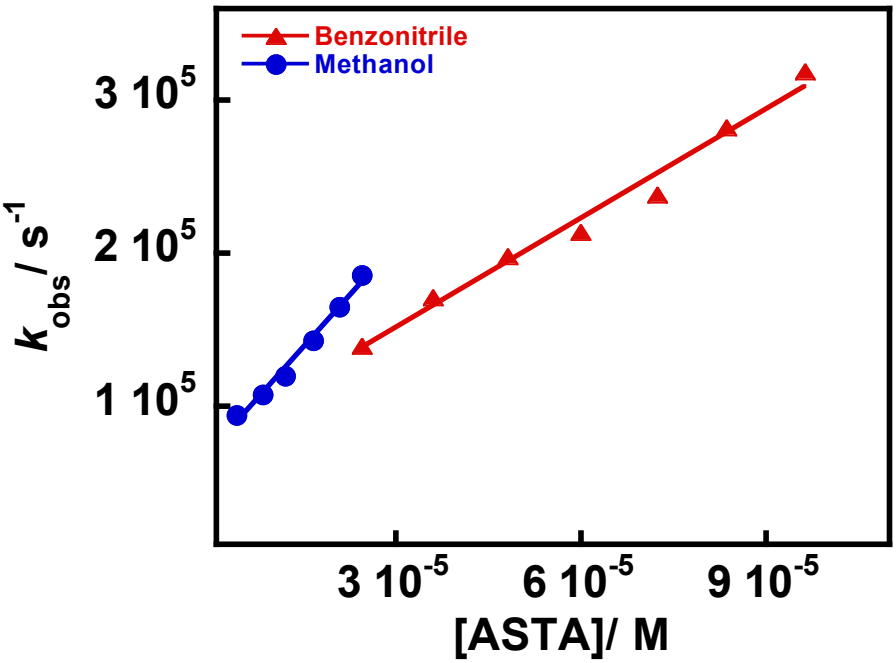

Fig. S23 Plots of pseudo-first-order rate constants (k_{obs}) for the decay of the transient profiles at 580 nm, obtained following LFP (355 nm) of retinol (4.5×10^{-5} M) in air-saturated methanol (laser energy ~10 mJ) or benzonitrile (laser energy ~25 mJ), *versus* ASTA concentration.

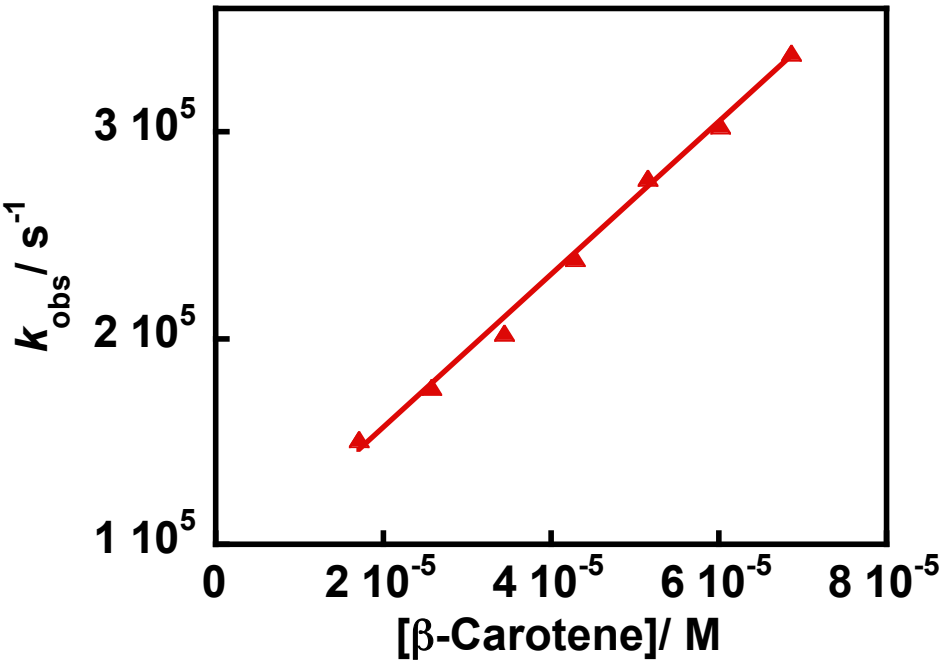

Fig. S24 Plot of pseudo-first-order rate constants (k_{obs}) for the decay of the transient profiles at 580 nm, obtained following LFP (355 nm) of retinol (4.5×10^{-5} M) in air-saturated benzonitrile (laser energy ~40 mJ), *versus* β-CAR concentration.

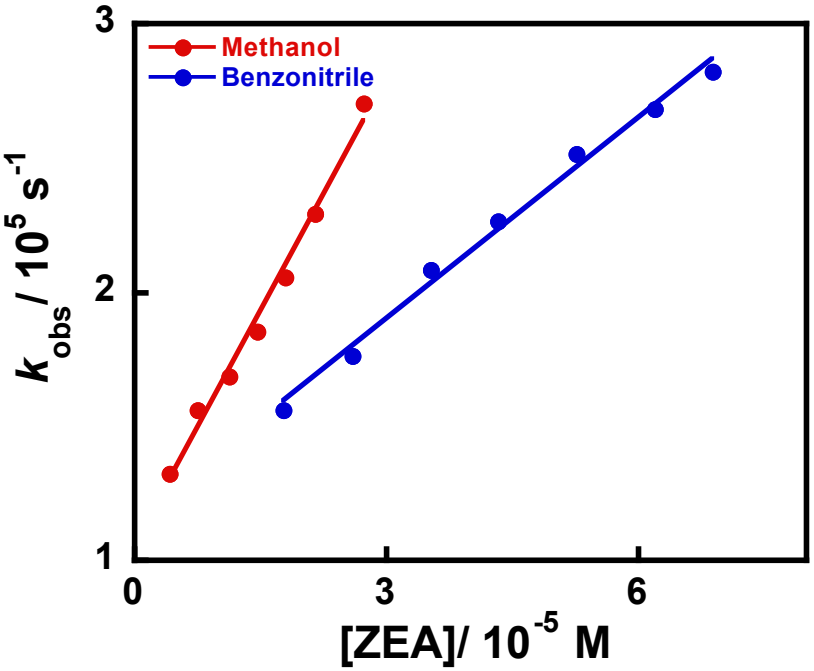

Fig. S25 Plots of pseudo-first-order rate constants (k_{obs}) for the decay of the transient profiles at 580 nm, obtained following LFP (355 nm) of retinol (4.5×10^{-5} M) in air-saturated methanol (laser energy ~20 mJ) or benzonitrile (laser energy ~30 mJ), *versus* ZEA concentration.

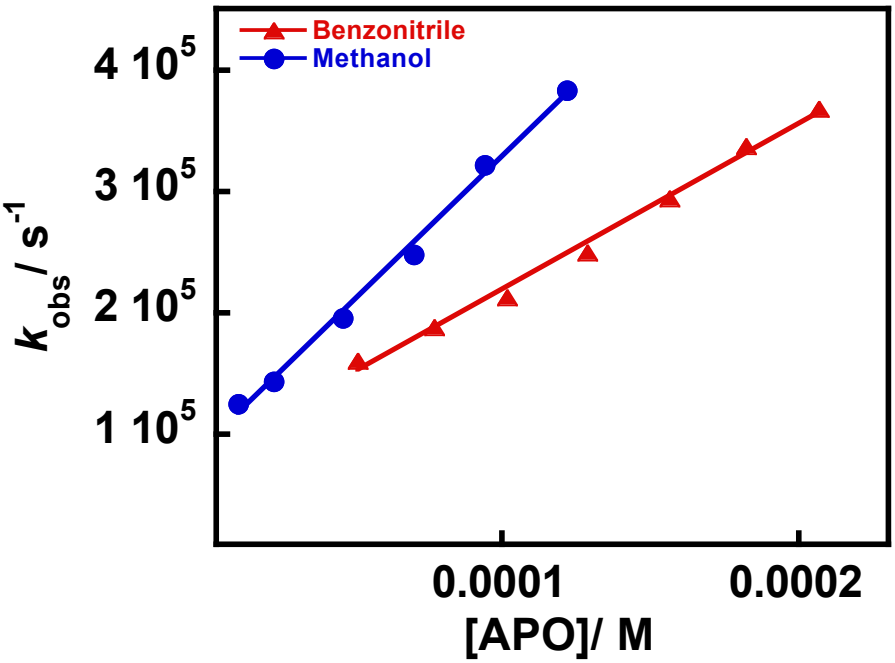

Fig. S26 Plots of pseudo-first-order rate constants (k_{obs}) for the decay of the transient profiles at 580 nm, obtained following LFP (355 nm) of retinol (4.5×10^{-5} M) in air-saturated methanol (laser energy ~15 mJ) or benzonitrile (laser energy ~30 mJ), *versus* APO concentration.

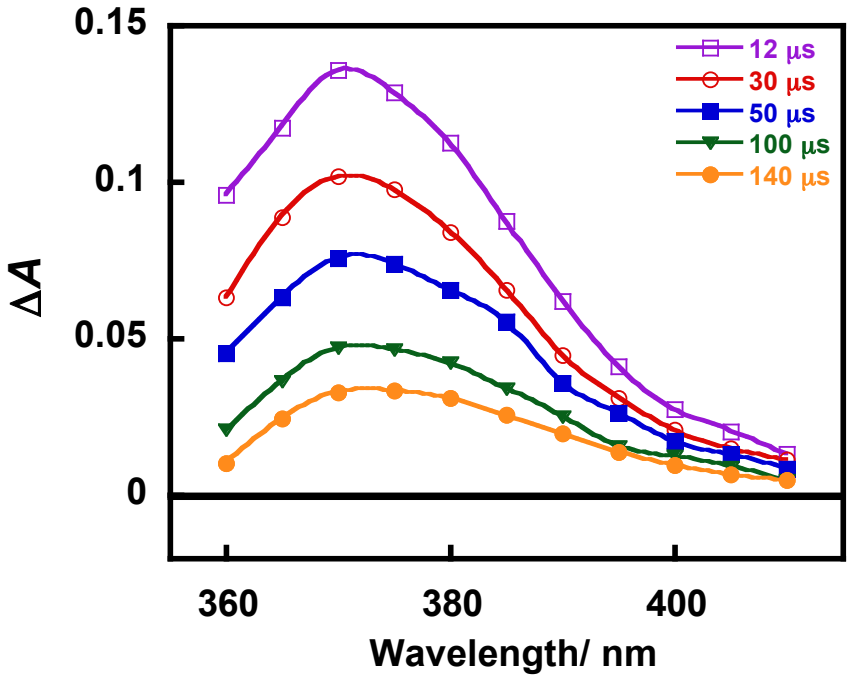

Fig. S27 Transient spectra obtained following LFP (355 nm) of retinol (4.5×10^{-5} M) and pyridine (1.0 M) in air-saturated methanol (laser energy ~15 mJ).

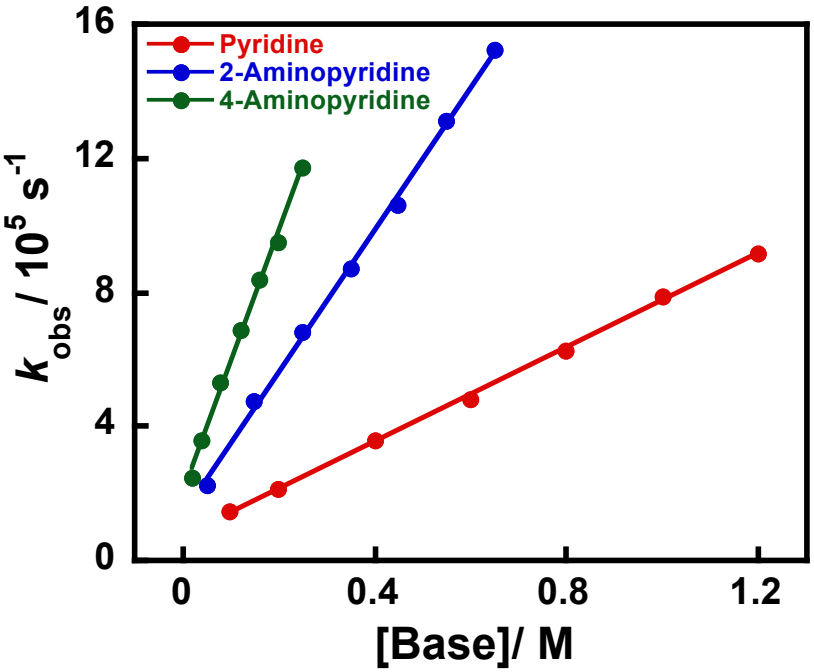

Fig. S28 Plots of pseudo-first-order rate constants (k_{obs}) for the decay of the transient profiles at 580 nm, obtained following LFP (355 nm) of retinol (4.5×10^{-5} M) in air-saturated methanol (laser energy ~20 mJ), *versus* pyridine derivative concentration.

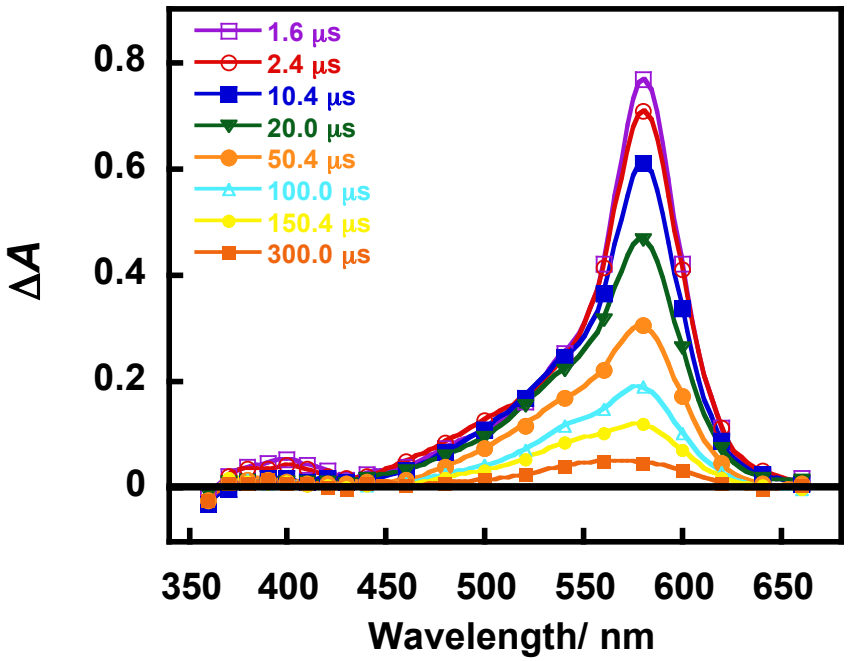

Fig. S29 Transient absorption spectra obtained following LFP (355 nm) of retinol (~1.0 × 10^{-4} M) in air-saturated aqueous 2% Triton X-100 (laser energy ~15 mJ).

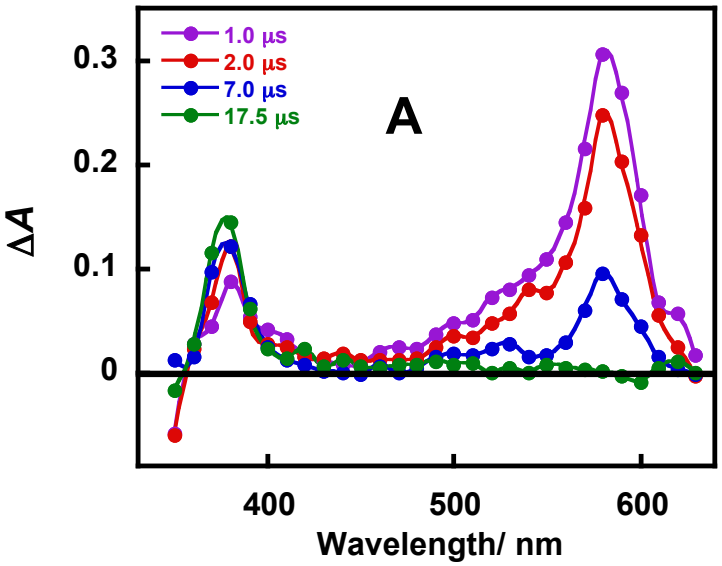

Fig. S30A Transient absorption spectra obtained following LFP (355 nm) of retinol (4.5×10^{-5} M) and pyridine (1.0 M) in air-saturated aqueous 2% Triton X-100 (laser energy ~20 mJ).

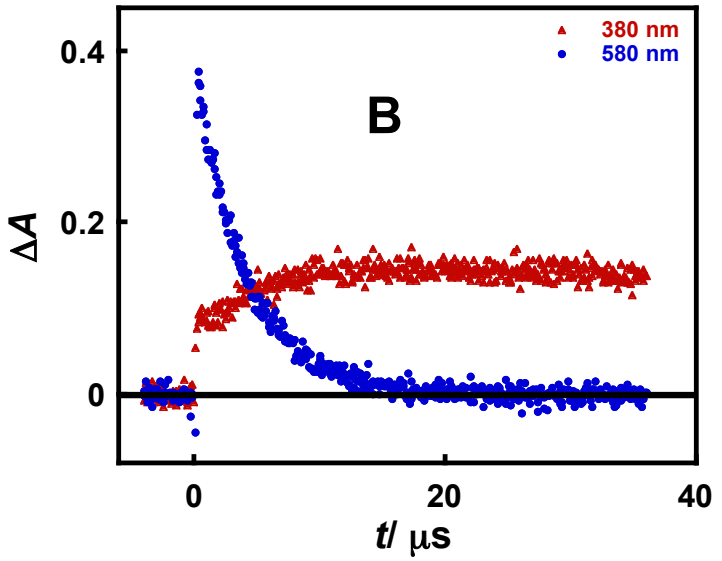

Fig. S30B Time profiles of absorbance at 580 and 380 nm obtained following LFP (355 nm) of retinol (4.5×10^{-5} M) and pyridine (1.0 M) in air-saturated aqueous 2% Triton X-100 (laser energy ~20 mJ).

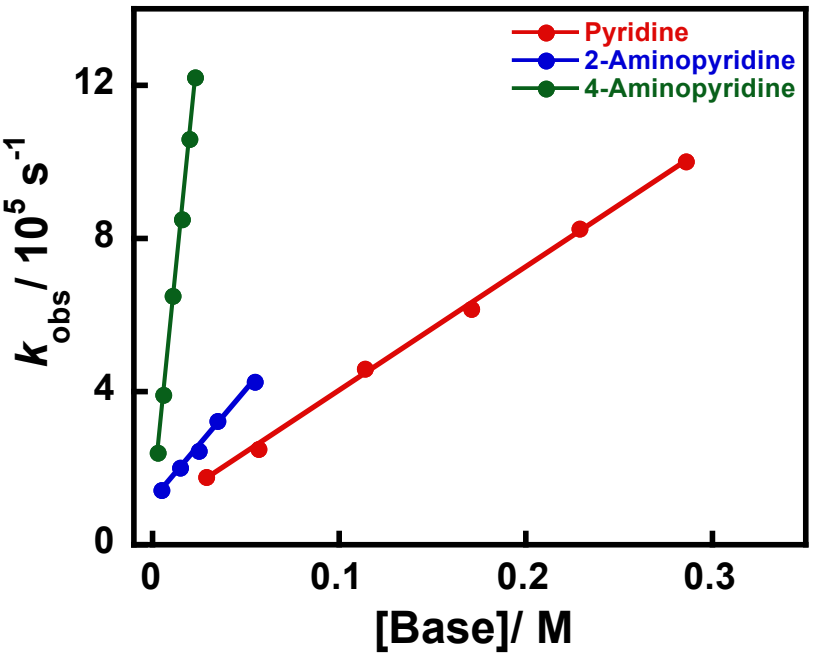

Fig. S31 Plots of pseudo-first-order rate constants (k_{obs}) for the decay of the absorbance at 580 nm, obtained following LFP (355 nm) of retinol (4.5×10^{-5} M) in air-saturated benzonitrile (laser energy ~25 mJ), *versus* pyridine derivative concentration.

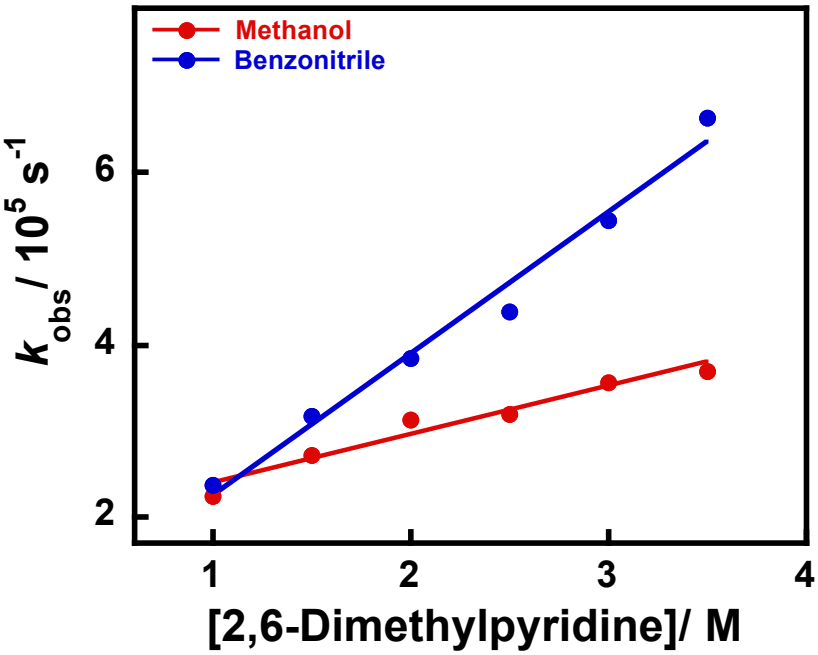

Fig. S32 Plots of pseudo-first-order rate constants (k_{obs}) for the decay of the absorbance at 580 nm, obtained following LFP (355 nm) of retinol (4.5×10^{-5} M) in air-saturated methanol (laser energy ~10 mJ) or benzonitrile (laser energy ~20 mJ), *versus* 2,6-dimethylpyridine concentration.

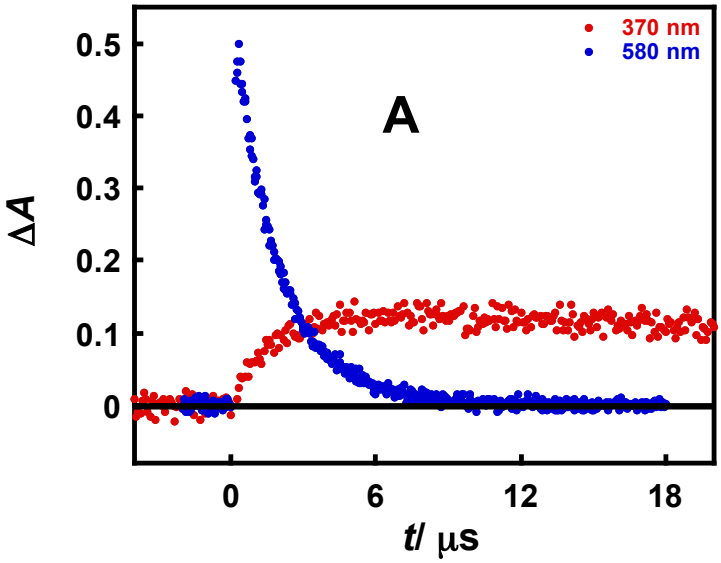

Fig. S33A Time profiles of absorbance at 580 and 370 nm obtained following LFP (355 nm) of retinol (4.5×10^{-5} M) and 2-aminopyridine (0.2 M) in air-saturated methanol (laser energy ~20 mJ).

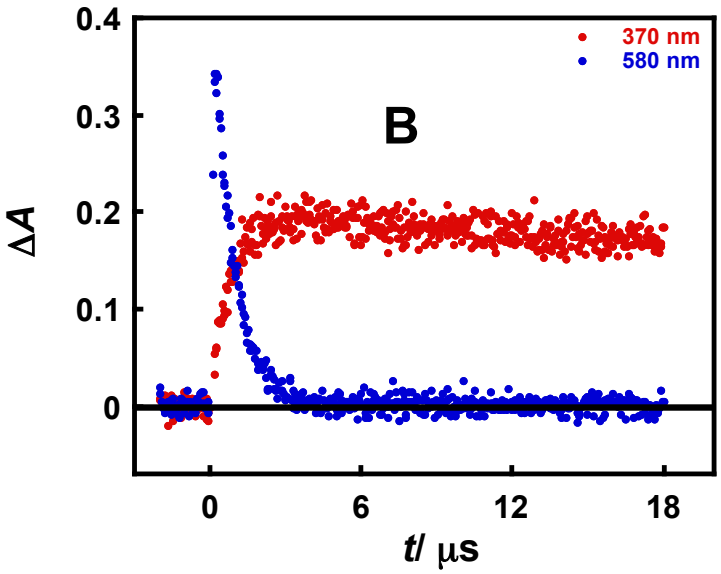

Fig. S33B Time profiles of absorbance at 580 and 370 nm obtained following LFP (355 nm) of retinol (4.5×10^{-5} M) and 4-aminopyridine (0.25 M) in air-saturated methanol (laser energy ~20 mJ).

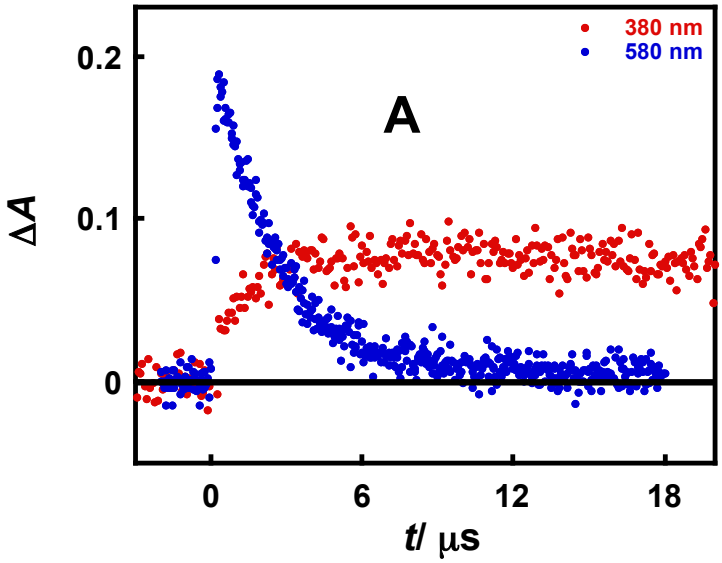

Fig. S34A Time profiles of absorbance at 580 and 380 nm obtained following LFP (355 nm) of retinol (4.5×10^{-5} M) and 2-aminopyridine (0.06 M) in air-saturated benzonitrile (laser energy ~20 mJ).

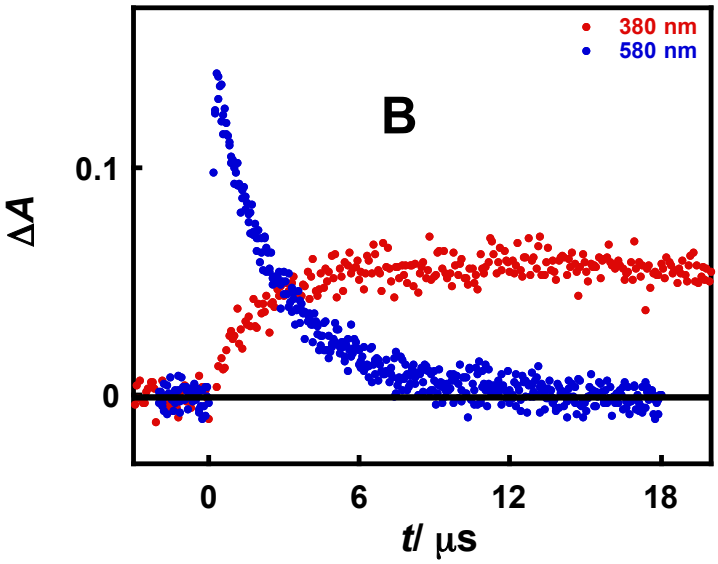

Fig. S34B Time profiles of absorbance at 580 and 380 nm obtained following LFP (355 nm) of retinol (4.5×10^{-5} M) and 2,6-dimethylpyridine (2.0 M) in air-saturated benzonitrile (laser energy ~20 mJ).

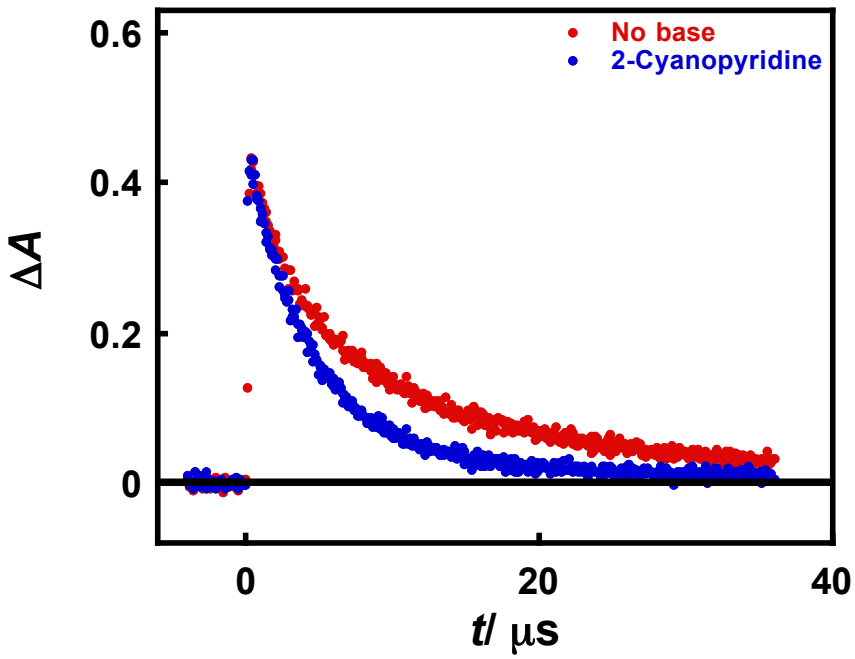

Fig. S35 Time profiles of absorbance at 580 nm obtained following LFP (355 nm) of (a) retinol (4.5×10^{-5} M) or (b) retinol (4.5×10^{-5} M) and 2-cyanopyridine (1.0 M) in air-saturated methanol (laser energy ~20 mJ).

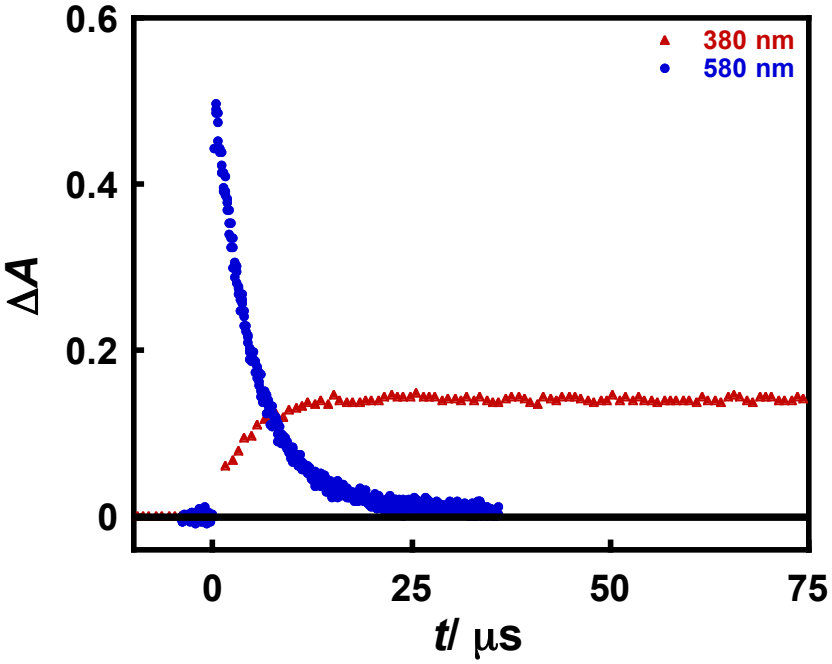

Fig. S36 Time profiles of absorbance at 580 and 380 nm obtained following LFP (355 nm) of retinol (4.5×10^{-5} M) in air-saturated aqueous 2% Triton X-100 at pH = 10.5 (laser energy ~25 mJ).

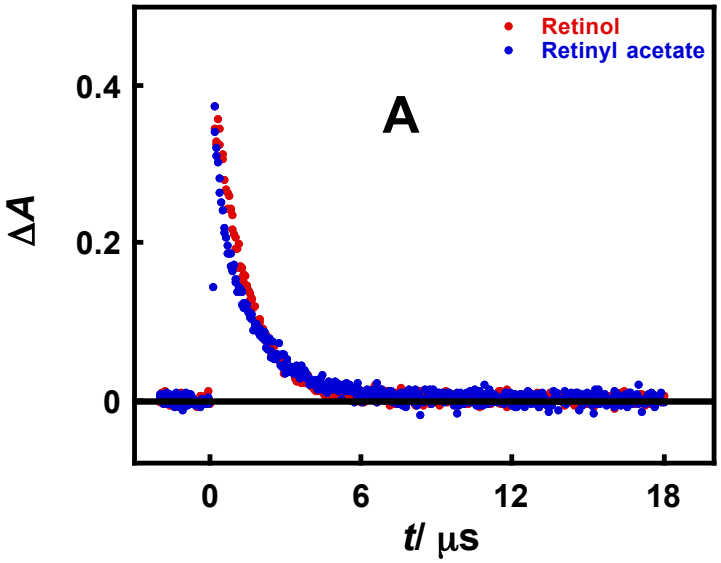

Fig. S37A Normalized time profiles of absorbance at 580 nm obtained following LFP (355 nm) of retinol (4.5×10^{-5} M) and retinyl acetate (Abs. at 355 nm ~0.8 in a 1 cm cell) in the presence of pyridine (1.0 M) in air-saturated methanol (laser energy ~15 mJ).

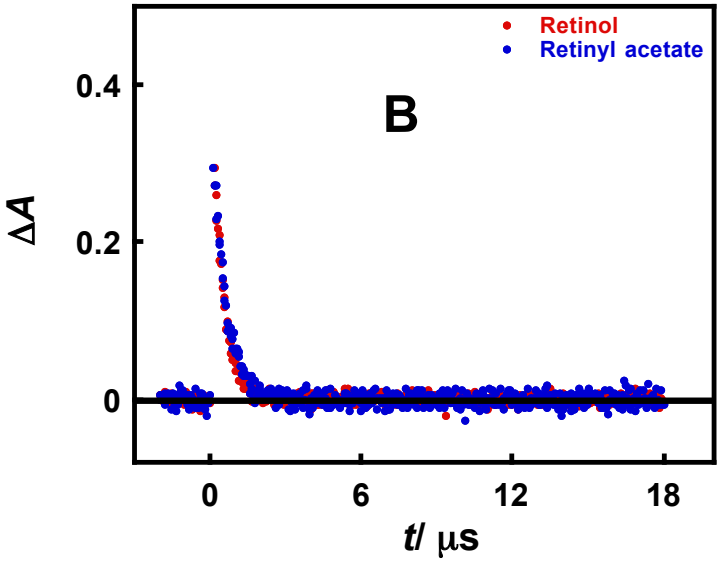

Fig. S37B Normalized time profiles of absorbance at 580 nm obtained following LFP (355 nm) of retinol (4.5×10^{-5} M) and retinyl acetate (Abs. at 355 nm ~0.8 in a 1 cm cell) in the presence of pyridine (1.0 M) in air-saturated acetonitrile (laser energy ~15 mJ).

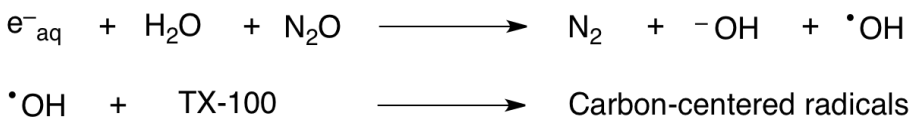

Scheme S1

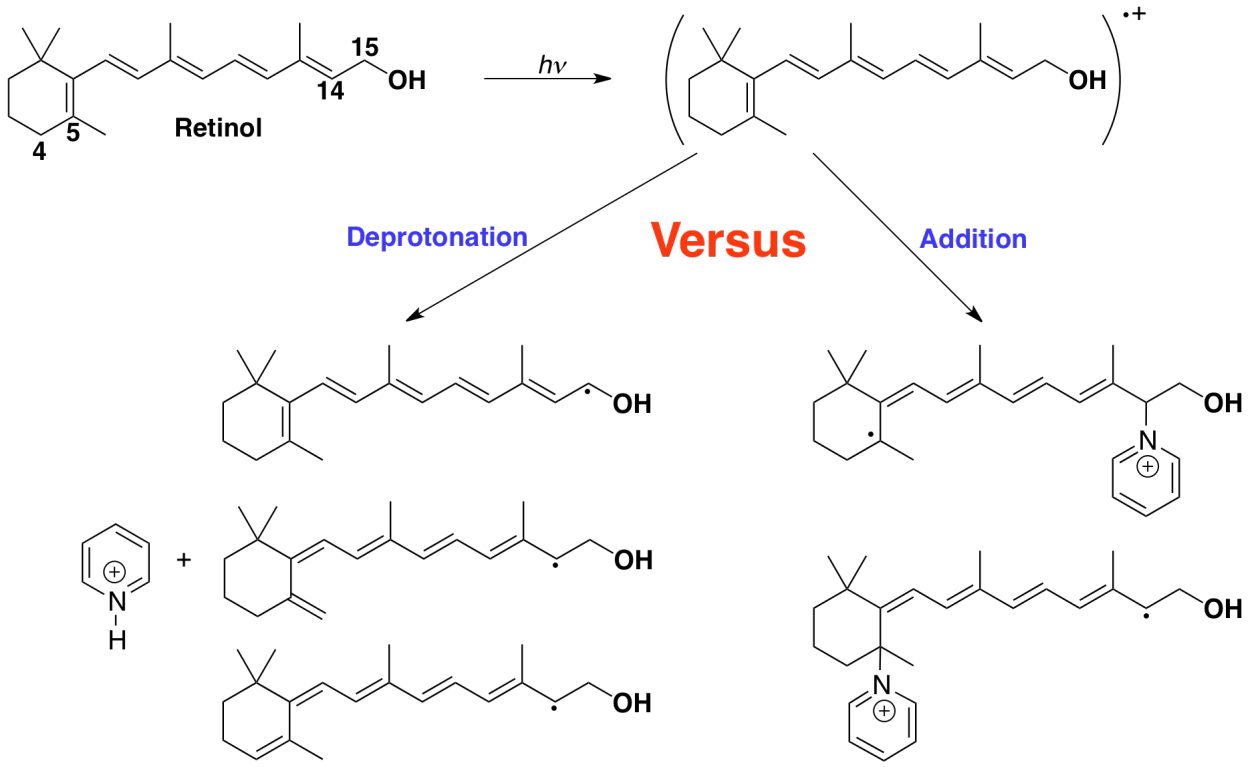

Scheme S2